Cell

Functional sensory circuits built from neurons of two species

Graphical abstract

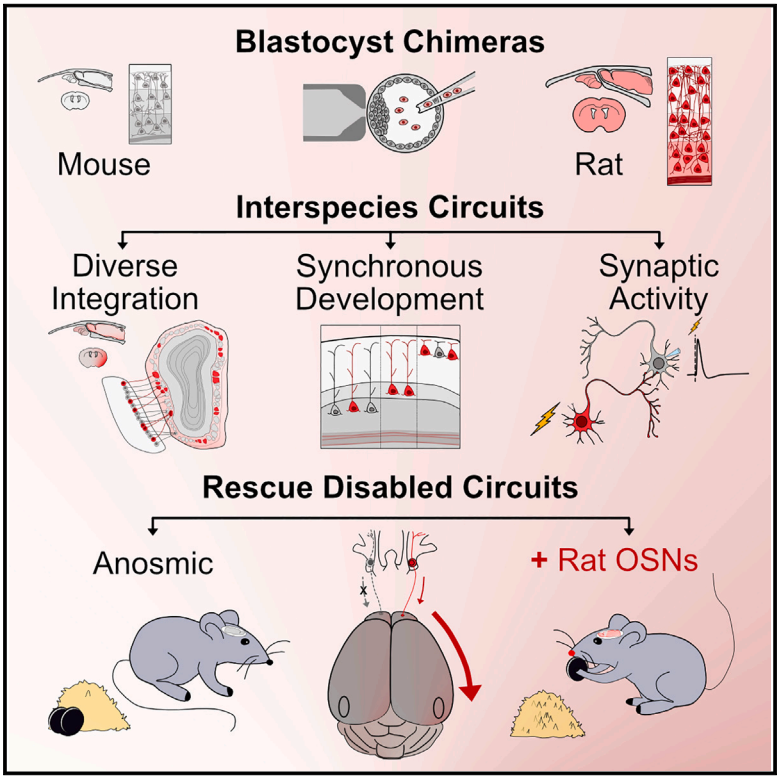

Highlights

- Rat stem cells develop in mouse blastocysts to broadly populate two-species brains
- Rat neurons develop synchronously and synapse with cognate mouse neurons
- Genetic models of circuit loss or silencing unveil rescue capacity of exogenous neurons
- Rat sensory neurons restore the primal behavior of food seeking to anosmic mice

Authors

Benjamin T. Throesch, Muhammad Khadeesh bin Imtiaz, Rodrigo Muñoz-Castañeda, ..., Juan Carlos Izpisua Belmonte, Jun Wu, Kristin K. Baldwin

Correspondence

kb238@columbia.edu (K.K.B.), jun2.wu@utsouthwestern.edu (J.W.)

In brief

Generating brains from two different species via blastocyst complementation enables synchronous development of appropriate interspecies circuits. When host sensory neurons are disabled, donor neurons restore a primal odor-driven food-seeking behavior, showing that one species can sense and respond to the world through the cognate neurons of another.

Throesch et al., 2024, Cell *187*, 2143–2157
April 25, 2024
https://doi.org/10.1016/j.cell.2024.03.042

CellPress

Cell

CellPress

Article

Functional sensory circuits built from neurons of two species

Benjamin T. Throesch,[1,2,13] Muhammad Khadeesh bin Imtiaz,[11,13] Rodrigo Muñoz-Castañeda,[3] Masahiro Sakurai,[4,5] Andrea L. Hartzell,[1] Kiely N. James,[1,2] Alberto R. Rodriguez,[6] Greg Martin,[6] Giordano Lippi,[1] Sergey Kupriyanov,[6] Zhuhao Wu,[7] Pavel Osten,[3] Juan Carlos Izpisua Belmonte,[4,9,10] Jun Wu,[4,5,8,11,*] and Kristin K. Baldwin[1,2,12,14,*]

[1]Department of Neuroscience, The Scripps Research Institute, La Jolla, San Diego, CA, USA
[2]Neuroscience Graduate Program, University of California, San Diego, La Jolla, San Diego, CA, USA
[3]Cold Spring Harbor Laboratory, Cold Spring Harbor, NY, USA
[4]Salk Institute for Biological Studies, La Jolla, San Diego, CA, USA
[5]Department of Molecular Biology, University of Texas Southwestern Medical Center, Dallas, TX, USA
[6]Mouse Genetics Core, The Scripps Research Institute, La Jolla, San Diego, CA, USA
[7]Icahn School of Medicine at Mount Sinai, New York, NY, USA
[8]Hamon Center for Regenerative Science and Medicine, University of Texas Southwestern Medical Center, Dallas, TX, USA
[9]Gene Expression Laboratory, Salk Institute for Biological Studies, La Jolla, San Diego, CA, USA
[10]Altos Labs, San Diego, CA, USA
[11]Cecil H. and Ida Green Center for Reproductive Biology Sciences, University of Texas Southwestern Medical Center, Dallas, TX, USA
[12]Department of Genetics and Development, Columbia Stem Cell Initiative, Columbia University Medical Center, New York, NY, USA
[13]These authors contributed equally
[14]Lead contact
*Correspondence: kb238@columbia.edu (K.K.B.), jun2.wu@utsouthwestern.edu (J.W.)
https://doi.org/10.1016/j.cell.2024.03.042

SUMMARY

A central question for regenerative neuroscience is whether synthetic neural circuits, such as those built from two species, can function in an intact brain. Here, we apply blastocyst complementation to selectively build and test interspecies neural circuits. Despite approximately 10–20 million years of evolution, and prominent species differences in brain size, rat pluripotent stem cells injected into mouse blastocysts develop and persist throughout the mouse brain. Unexpectedly, the mouse niche reprograms the birth dates of rat neurons in the cortex and hippocampus, supporting rat-mouse synaptic activity. When mouse olfactory neurons are genetically silenced or killed, rat neurons restore information flow to odor processing circuits. Moreover, they rescue the primal behavior of food seeking, although less well than mouse neurons. By revealing that a mouse can sense the world using neurons from another species, we establish neural blastocyst complementation as a powerful tool to identify conserved mechanisms of brain development, plasticity, and repair.

INTRODUCTION

The genome is the ultimate architect of the brain. Its evolutionary variations enable the precise assembly of diverse cellular subtypes into neural circuits with species-specific functions. For example, mammals such as bats and dolphins have evolved new senses such as echolocation. Other species have become specialized to rely on a particular sense, such as smell for mice, vision for primates, or touch for blind mole rat species that live underground. How the genetic differences that arise between species produce the remarkable diversity of neural functions that occur in nature remains a fundamental question for evolution, genomics, and neuroscience.

Further, an ultimate goal for regenerative medicine is to form "synthetic" neural circuits that can rescue or augment the function of damaged or degenerating brains. Newly developing approaches for this include within-brain reprogramming or *trans*-differentiation, selective neural transplantation, or machine-brain interfaces. Understanding how neural plasticity may overcome interspecies differences in brain size, developmental timing, cell-type composition, circuit structure, and even behavioral capacities can provide insights to inform efforts to restore brain function in developmental disorders, aging, and degenerative disease.

To investigate these questions, we set out to build and functionally test "synthetic" neural circuits derived from neurons of two species, in an intact brain. To accomplish this, we applied blastocyst chimera methods in which we injected pluripotent stem cells (PSCs) of one species into the developing blastocyst of a genetically divergent host. This produces chimeric organisms with broad and generally stochastic contribution across tissues, as previously reported.[1–5] Blastocyst chimeras can also be

modified to allow donor cells to replace entire organs or cell types by generating an empty niche, termed blastocyst complementation. This approach has long been successfully applied in the hematopoietic system and recently has been extended to other systems, for example, to study cortical development in mouse-mouse chimeras where developing host neurons are killed early in development.[6–11]

Here, we establish robust methods for selective neural blastocyst complementation. We use mouse blastocysts as hosts and either rat PSCs or genetically distinct mouse strains as donors. Host niches are selectively depleted by genetic killing or synaptically silenced by expressing a neurotoxin in specific neuronal cell types. In these interspecies brain chimeras, rat cells develop synchronously with mouse neurons, integrate widely in neural circuits throughout the wild-type (WT) mouse brain, and form active synaptic connections with mouse neurons. When mouse olfactory sensory neurons (OSNs) are killed or silenced, rat replacement neurons rescue olfactory circuit anatomy, participate in information transfer, and can partly restore food-seeking behavior. However, rat neurons perform differently at each level of function, depending on whether mouse cells are absent, or they are present but silent. By demonstrating the capacities and limitations of selective neural blastocyst complementation, we validate two platforms to probe evolutionarily conserved mechanisms governing neural circuit function and repair. Future refinements may extend these neural complementation methods to encompass additional neural circuits, more complex behaviors, and increasingly distant species.

RESULTS

Quantitative whole-brain imaging of rat-mouse chimeras

Some mouse brain regions may be more amenable to rat complementation than others, which has implications for the utility of neural blastocyst complementation. We generated interspecies chimeras using a rat embryonic stem cell (ESC) line (DAC2)[12] that expresses a bright red-orange fluorescent protein, Kusabira Orange (KsO).[3] We injected these ESCs into mouse blastocysts, which were then transferred into the uteri of surrogate mouse mothers to complete their development (Figure 1A; Table 1). Rat-mouse chimeras exhibited varying rat cell contribution based on KsO fluorescence (Figure 1A). Chimeras showed non-symmetric, bilateral patterning of neural cells across brain regions including the olfactory bulbs (OBs), piriform cortex (PCx), multiple neocortical areas, hippocampus (Hipp), caudoputamen (CP), and cerebellum (CB) (Figure 1B). Within each region, rat neurons displayed diverse yet regionally characteristic cellular morphologies and layering (Figure 1B). KsO signal was also found in non-neuronal cell types such as microglia, astrocytes, and vascular cells. We quantified the average neuronal contribution per region, by measuring the percent of KsO (rat cells) that expressed NeuN (neurons from either mouse or rat) throughout 7 brain regions from 4 to 7 mice per region. Astrocytes and microglia were scored based on morphology and absence of NeuN (Figure 1C). These regions in the chimeras did not have detectable rat vascular contribution. We found that between ~40% and 90% of KsO cells were NeuN-positive neurons across all regions and mice, indicating that whole-brain imaging analyses would be informative regarding the potential for neuronal contribution to different brain regions (Figure 1D).

We analyzed the extent and location of rat cells across the entire brain using light-sheet microscopy and whole-brain clearing (n = 6 chimeras) (Figures 1E and S1A–S1D). We quantified this by developing a method for registration and quantification of the percent KsO signal per volume for any defined three-dimensional brain region and presented this in a flat map representation (Figure S1C). Rat brain contribution is broad yet variable among chimeras and differs between two hemispheres of the same animal, consistent with the stochastic contribution patterns of same-species chimeras (Figures S1C and S1D). Mapping red rat cells to the Developing Mouse Brain Reference Atlas (Figure 1F) and the Allen Mouse Brain Reference Atlas (Figure S1E) showed that concordance between regions and rat contribution was more apparent in the developmentally defined regions than in the adult anatomic regions. Most brain regions had a detectable rat signal (KsO) ranging from 0.01% to 87.12%, (Figure 1F; Table 1). The most consistent significant trend was a reduced contribution to the pallium and subpallium (Figure 1F). We confirmed that the red neuronal cells were indeed derived from our rat PSCs using RT-PCR and sequencing for a neuronal gene (synapsin 1) carrying a polymorphic deletion in the rat vs. the mouse. We detected both rat and mouse contribution in cortical and OB brain tissues from 3/3 chimeras (Figure S1F).

Reprogramming of rat neuronal birth dates

A main evolutionary distinction between brains of different species is the timing of differentiation of cognate neuronal subtypes. For example, rat brains are larger than mouse brains, with expanded cortical layers, and cognate cortical neurons develop roughly 1 to 2 days later than the mouse.[13] This is a question of high significance for the use of interspecies brain models and is likely informative for transplantation efforts.

Specifically, we predict that if xenogeneic cells adapt to the developmental timing of the host species, this would enable more precise formation and function of the rescued or reconstituted neuronal circuits. However, decades of cross-species tissue grafting experiments have shown that in most contexts, transplanted cells maintain their own species-specific developmental timing despite maturing in an accelerated host environment.[14–17] In contrast, recent heterochronic intraspecies transplantation studies have shown that some mouse cortical progenitor populations retain the capacity to read the host mouse cues and adapt to their environments.[18] Here, we sought to determine whether rat neurons developing in tandem with mouse cells from the earliest stages of embryogenesis would differ from grafting experiments and be able to successfully interpret extracellular timing cues resulting in host-based "reprogramming" of donor birth dates.

To examine these possibilities, we birth dated rat neurons using bromodeoxyuridine (BrdU) and 5-ethynyl-2'-deoxyuridine (EdU) injections at several time points (from E12.5 to E17.5) where birth dates of mouse and rat cells differ (Figure 2A). Cortical regions comprise multiple layers built by radial migration from the ventricular zone such that early-born neurons are

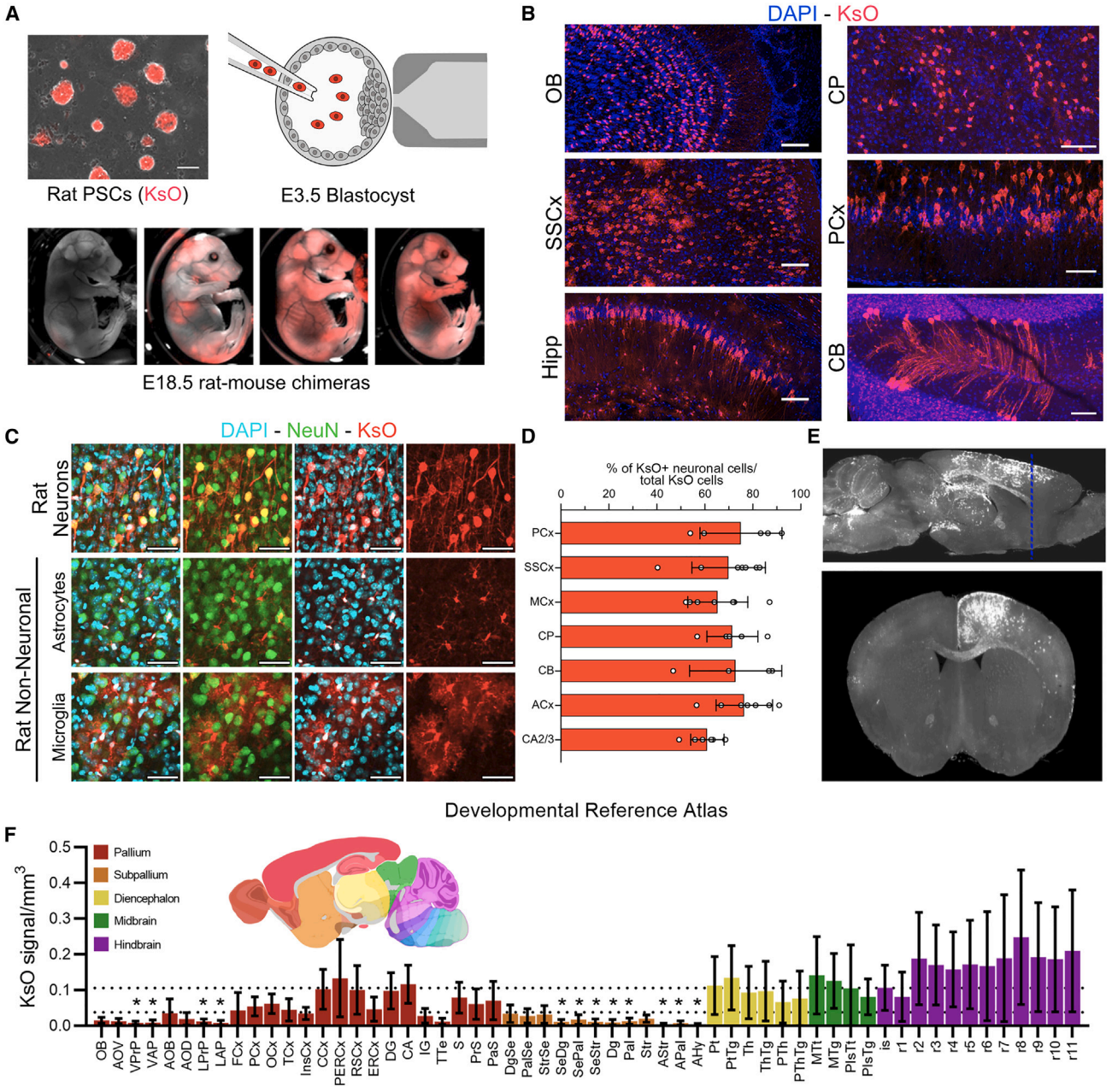

Figure 1. Rat cells contribute widely to the mouse brain

(A) Schematic of rat-mouse chimera formation. Rat pluripotent stem cells (PSCs) labeled with KsO (red) were injected into E3.5 mouse blastocysts. Derived E18.5 fetuses displayed variable KsO contribution.

(B) Rat contribution to diverse neural circuits; nuclei (DAPI, blue) and rat KsO cells (red). OB, olfactory bulb; PCx, piriform cortex; SSCx, somatosensory cortex; CP, caudoputamen; Hipp, hippocampus; CB, cerebellum. Scale bars, 100 μm.

(C) Rat contribution to neuronal and non-neuronal cell populations; nuclei (DAPI [cyan]), neurons, NeuN (green), and rat KsO (red). Scale bars, 50 μm.

(D) Quantification of rat contribution. Shown are the mean ± 95% CI. Animals analyzed per brain region; PCx = 5, SSCx = 7, MCx = 7, CP = 5, CB = 4, ACx = 7, and CA2/3 = 7.

(E) Whole-brain imaging of high-contribution chimeric brains (KsO, white).

(F) Volumetric analysis based on the Allen Developing Mouse Brain Reference Atlas. Results of 12 hemispheres from 6 independent brain samples are shown, mean ± 95% CI. Dashed lines indicate the 95% CI for the mean hemisphere signal. Significance was tested by repeated measures one-way ANOVA with Dunnett's multiple comparisons test to the mean hemisphere signal, $^{*}p < 0.05$, $^{**}p < 0.01$.

See also Figure S1.

Table 1. Blastocyst complementation efficiencies

Rat PSC line	Mouse strain	Blastocysts injected	Total pups	Total chimeras	% Chimera/Blast.	% Chimera/live birth
DAC2 ESC	total	3,651	791	256	7%	32%
DAC2 ESC	WT	630	105	56	9%	53%
DAC2 ESC	Silence	1,912	333	85	4%	26%
DAC2 ESC	Ablate	1,109	353	115	10%	33%
DAC8 ESC	Ablate	234	44	2	1%	5%
SD riPSC 9.3	WT	120	53	22	18%	42%

Summary and efficiencies of blastocyst injections of different rat PSCs into different mouse genetic backgrounds (Ablate, Silence, or wild type [WT]). Rat lines DAC2 and DAC8 express Kusabira Orange (KsO) in all cells. Rat line SD riPSC 9.3 was an iPSC line generated in the Baldwin lab from rat fibroblasts and expresses YFP fused to channelrhodopsin-2 driven by the human synapsin promoter based on a lentiviral integration into iPSCs and clonal selection.

located in deep layers, and later-born neurons migrate further to build superficial layers.[19,20] If rat neurons maintain their species-intrinsic clock, EdU labeling should show a difference in the layering of mouse and rat neurons in the same chimeric brain, where rat neurons are in deeper (less mature) layers based on their longer developmental time frame (Figure 2A). Alternatively, if donor (rat) neurogenesis is reprogrammed by the host mouse developmental niche, rat neurons should be intermingled spatially with mouse neurons born on the same day (Figure 2A).

Analyses of three cortical regions across three time points showed the same striking result; in all regions and time points, rat neurons developing in the mouse brain adopt the developmental timing of the host, as shown by intermixing of mouse and rat cells in each layer (Figures 2B and 2C) and co-expression of the layer IV and V marker CTIP2 (Bcl11b) (Figures S2A and S2B). As a control for sensitivity, we show that the assay is sensitive enough to detect a single day's difference in birth date, using control comparisons of mouse (and rat) cells born on E13.5 vs. E14.5 (Figures 2B and 2C). Similar findings emerged from other brain regions (Hipp CA1, PCx layer 2, and CP), using double labeling with BrdU at E12.5 and EdU at either E13.5 or E14.5 (Figure 2D). We did detect a very small but statistically significant reduction in the earliest born rat neurons in the subpallial region (CP) (Figure 2D). This is consistent with the lower overall contribution of rat cells to subpallial regions in the whole-brain imaging studies (Figure 1F). The results illustrate that developmental timing of xenogeneic donor PSC-derived neurons can usually be reprogrammed, strongly implicating non-cell-autonomous mechanisms specific to the host. This result contrasts with historical grafting and transplantation studies, suggesting that this reprogramming occurs at early developmental stages. This concurs with results from other interspecies chimeras in which the host environment governs the body and organ size, as well as the development of a chimeric organ absent from the donor species (gall bladder).[3,5,7]

Rat neurons synapse with mouse neurons

Neurons relay information through synaptic neurotransmission. However, neurons from different species may differ in proteins or signaling molecules necessary to recognize and form connections with synaptic partners *in vivo*.[21] To rigorously test interspecies synapse formation, we generated and validated a rat induced pluripotent stem cell (iPSC) line expressing the human channelrhodopsin carrying the H134R mutation and fused to enhanced yellow fluorescent protein (eYFP) (hChR2(H134R)-eYFP)[22] under control of the human synapsin promoter (hSyn) (riPSC::hSyn-ChR2-eYFP) (Figures 3A, S3A, and S3B). In chimeras made from this line, rat cells express eYFP, appear yellow, and can be activated to depolarize and release synaptic vesicles when blue light is present. Chimeras with rat contributions in cortical and hippocampal regions were readily produced from hSyn-ChR2-eYFP iPSCs (Table 1). To detect interspecies synapses, we collected acute slices containing the Hipp and cortex for electrophysiology recordings (Figure 3B). Recordings from mouse (eYFP negative) hippocampal and cortical pyramidal neurons in the region of optogenetic stimulation revealed excitatory postsynaptic potentials (EPSPs) in mouse neurons 5–15 ms after light stimulation that were blocked by AMPA and NMDA glutamate receptor antagonists (Figures 3B, 3C, S3C, and S3D). In contrast, recording directly from a eYFP-positive rat neuron while it was being stimulated evoked responses that were not blocked pharmacologically (Figure 3D). Comparisons of all recorded neurons show differences between the mouse neurons and the rat neurons in sensitivity to CPP/NBQX and in time of onset (Figure 3E). Therefore, rat neurons can form functional synapses with mouse neurons in the Hipp and cortex in circuits that appear spatially normal and arise at similar developmental stages.

Intraspecies circuit rescue in genetic models of sensory dysfunction

Human neural cell replacement therapies are envisioned for cases where neurons are missing due to injury or cell death or when they remain present but have lost the capacity for meaningful synaptic communication. Here, we test whether donor PSC-derived mouse and rat neurons can functionally complement genetic mouse models of (1) neural cell loss and (2) synaptic impairment, using the well-characterized and genetically tractable circuits of the olfactory system.

Odor sensation begins with OSNs found in the olfactory epithelium (OE) of the nose. OSNs are produced by basal stem cells in the OE throughout the life of an organism and are one of the few sites of adult neurogenesis (Figure 4A). Mature OSNs target their axons to one of two spatially invariant glomeruli in the OB, depending on their stochastic choice of 1 of ~1,200 genetically encoded olfactory receptors (ORs) (Figure 4A).[23,24] The general spatial position of glomeruli is

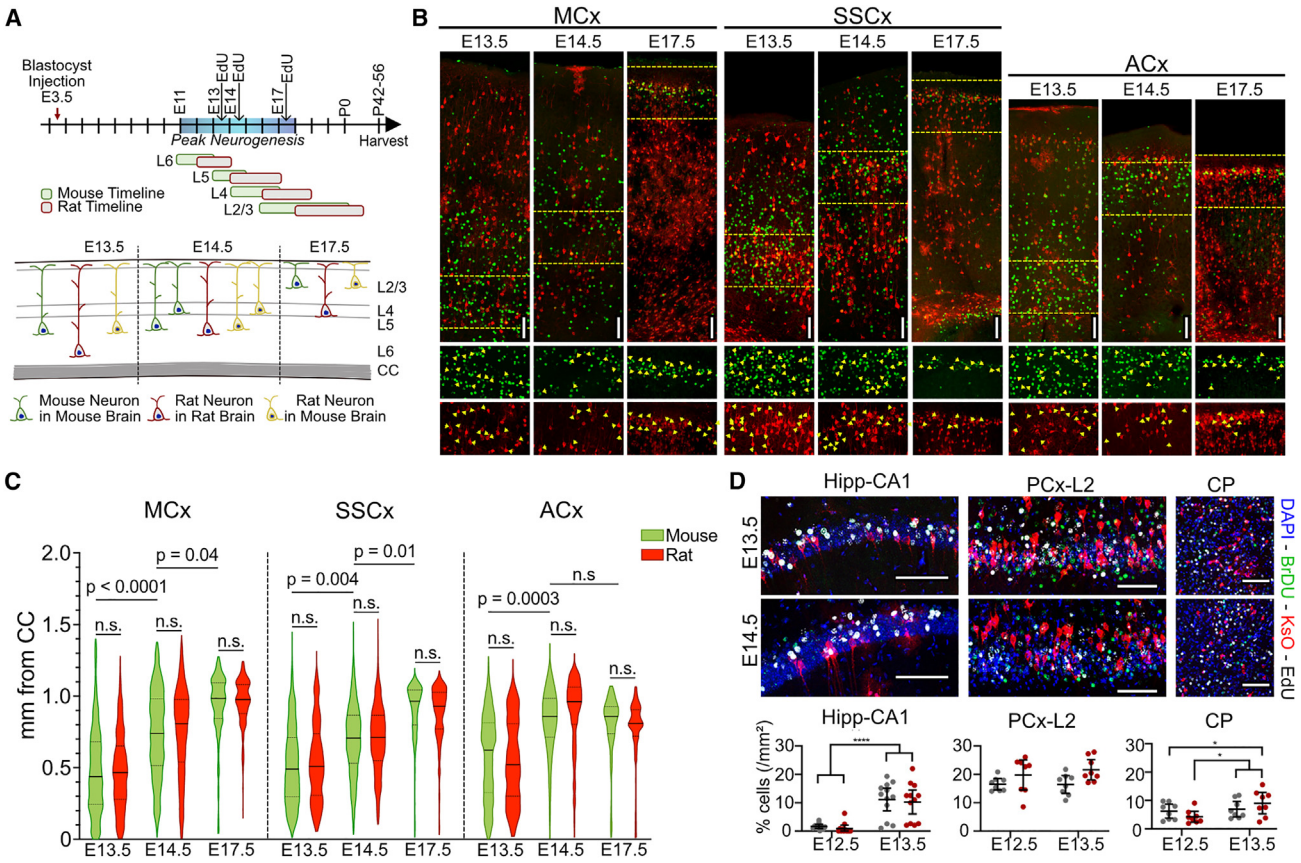

Figure 2. Development of rat cells within mouse neural circuits

(A) Schematic of birth-dating experiments. Surrogate mothers were injected with BrdU at E12.5 and with EdU at E13.5, E14.5, or E17.5 to label different populations of neurons in chimeric embryos during peak mouse neurogenesis. Rat neurons could either maintain their developmental timeline (red neurons) or reprogram their timeline to that of the mouse cells (yellow, matching mouse in green).

(B) EdU labeling at E13.5, E14.5, and E17.5 in 3 cortical regions, motor (MCx), somatosensory (SSCx), and auditory cortex (ACx). Rat KsO cells (red) and EdU-labeled cells (green). Scale bars, 100 μm.

(C) Distance of each cell from the border between the cortex and the corpus callosum (CC). Data shown are the median and the upper and lower quartiles for each time point and cortical region. Statistical tests comparing mouse and rat distances were multiple paired t tests, corrected by the Sídák method. Animals per time point: E13.5 = 3, E14.5 = 4, and E17.5 = 1. Number of sections: MCx E13.5 = 9, MCx E14.5 = 12, MCx E17.5 = 7, SSCx E13.5 = 9, SSCx E14.5 = 12, SSCx E17.5 = 10, ACx E13.5 = 9, ACx E14.5 = 12, and ACx E17.5 = 9. Number of cells per section = MCx, 2,138 cells (E13.5-mouse), 498 (E13.5-rat), 2,961 (E14.5-mouse), 387 (E14.5-rat), 524 (E17.5-mouse), and 376 (E17.5-rat); SSCx, 3,600 (E13.5-mouse), 644 (E13.5-rat), 5,220 (E14.5-mouse), 1,072 (E14.5-rat), 1,811 (E17.5-mouse), and 709 (E17.5-rat); ACx, 2,879 (E13.5-mouse), 673 (E13.5-rat), 3,568 (E14.5-mouse), 506 (E14.5-rat), 717 (E17.5-mouse), and 222 (E17.5-rat). *p values* = ACx E13.5, $p = 0.15$; ACx E14.5, $p = 0.62$; ACx E17.5, $p > 0.99$; MCx E13.5, $p > 0.99$; MCx E14.5, $p > 0.99$; MCx E17.5, $p > 0.99$; SSCx E13.5, $p = 0.13$; SSCx E14.5, $p = 0.58$; and MCx E17.5, $p = 0.65$. Significance tests comparing mouse distances across time points were performed using one-way ANOVA, corrected by the Šídák method.

(D) Rat temporal development is reprogrammed in mouse non-cortical regions. Top: BrdU (labeled E12.5) and EdU (labeled E13.5 or E14.5) staining in CA1 hippocampus (Hipp-CA1), layer 2 piriform cortex (PCx-L2), caudoputamen (CP). Nuclei (DAPI, blue), BrdU (green), rat KsO cells (red), and EdU (white). Scale bars, 100 μm. Bottom: data are mean ± 95% CI, $n = 3$–4 animals, 3 slices/animal. Significance was tested by two-way ANOVA and Sídák's multiple comparisons test, $^{*}p < 0.05$, $^{**}p < 0.01$, $^{***}p < 0.001$, and $^{****}p < 0.0001$.

See also Figure S2.

conserved and similar between mouse and rat,[25–27] but the rat genome encodes ~100 more ORs than the mouse genome, creating a larger OB with more glomeruli than in the mouse.[28] Olfactory information travels to cortical processing centers via the olfactory mitral and tufted (MT) neurons, which project ipsilaterally and are the only direct output of the OB. Therefore, the olfactory system allows us to successively test the capacity of donor cells to rescue successive stages of olfactory circuit formation, maintenance, and processing.

To this end, we established two distinct mouse models in which OSNs are either genetically disabled or killed. Mice with the Cre recombinase gene under the control of the endogenous olfactory marker protein (OMP) locus express Cre protein specifically in mature OSNs. These mouse lines are widely used to selectively mark and manipulate OSNs.[27–29] To selectively kill OSNs, we used this line to express diptheria toxin subunit A by crossing it to a floxed (DTA, "Ablate" model) (Figure 4A). To synaptically silence OSNs, we use Cre-activated, selective OSN

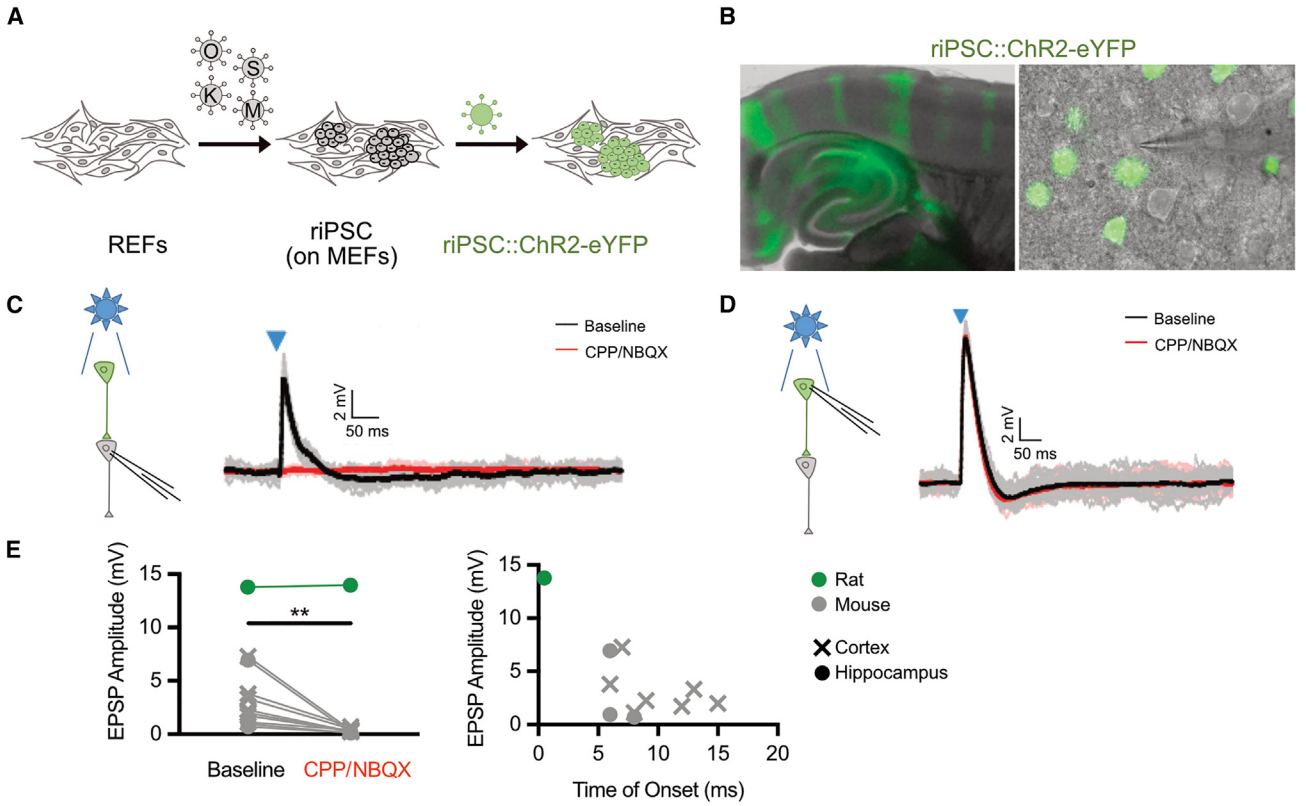

Figure 3. Rat neurons form functional synaptic connections with mouse neurons

(A) Schematic of rat iPSC reprogramming and ChR2-eYFP insertion. REF, rat embryonic fibroblast; riPSC, rat induced pluripotent stem cell; MEF, mouse embryonic fibroblast.

(B) Acute transverse slice images from 2- to 4-week-old chimera brains. Mouse cells were eYFP negative.

(C) Evoked EPSPs in a mouse neuron upon stimulation of rat neurons with blue light. Glutamate receptor antagonists (CPP, NBQX) abolished light-evoked depolarizations. Blue triangles mark blue light stimulation. Traces are an average of 20 trials. Scale bar is 2 mV, 50 ms.

(D) Recordings from rat neuron (YFP positive) upon light activation. Traces are an average of 20 trials. Scale bar is 2 mV, 50 ms.

(E) Peak EPSP amplitude ± glutamate receptor antagonist for rat (green) and mouse (gray) (left). EPSP amplitude vs. time of onset of the signal. Rat (green) and mouse (gray); cortex (cross) and hippocampus (circle) (right). n = 10 YFP− mouse cells, 1 YFP+ rat cell, 7 animals. Significance for mouse cells tested by two-tailed, paired t test. $^{**}p < 0.01$.

See also Figure S3.

expression of a floxed tetanus neurotoxin light chain (TeNT, "Silence" model) (Figure 4A).[27] DTA expression in Ablate mice kills mature OSNs (Figures S4A and S4B) resulting in a decreased glomerular layer area at P5 due to very few OSN axonal inputs to glomeruli in the OB (Figure 4B). In adult animals, a small number of misshapen glomeruli emerge in certain regions of the OB, perhaps due to regional escape from DTA expression (Figures S4C and S4D). However, in all chimeras, the OB size, glomerular layer, and individual glomerulus size are clearly reduced in the Ablate animals. In the Silence model, expression of TeNT in OSNs prevents neurons from releasing synaptic vesicles by cleaving the vesicular-associated membrane protein (VAMP), but it allows normal OB formation as reported previously and shown here (Figures 4A–4C).[27,30,31]

We tested whether intraspecies (mouse-mouse) neural blastocyst complementation approaches were effective in the olfactory system. In both the Silence and Ablate models, red (tdTomato-labeled) WT mouse PSC-derived neurons innervated the OE and projected axons to the OB. The donor mouse cells also rescued the anatomic aberrations in the OB of the Ablate mice (Figures 4D and 4E). We employed the buried cookie test to test whether WT mouse OSNs could restore function to these disabled circuits in a blastocyst complementation model.[32] In this well-established assay, animals are habituated to a food reward and rested for 4–5 days, and video monitoring is used to score the time to find a hidden cookie (Figure 4F). WT donor cells rescued the impaired cookie-finding behavior in both models (Figure 4G). However, the Silence non-chimeric littermates performed unusually well, compared with a similar cohort from the rat rescue experiments. This may reflect the larger litter size of the mouse-mouse chimera experiments that has been shown to reduce overall survival of anosmic mice and therefore may have selected for Silence mice with the best olfactory-mediated behavior (Figures 4G and S4E). Overall, rescue of sensory circuits and olfactory behavior is highly effective using same species neural blastocyst complementation.

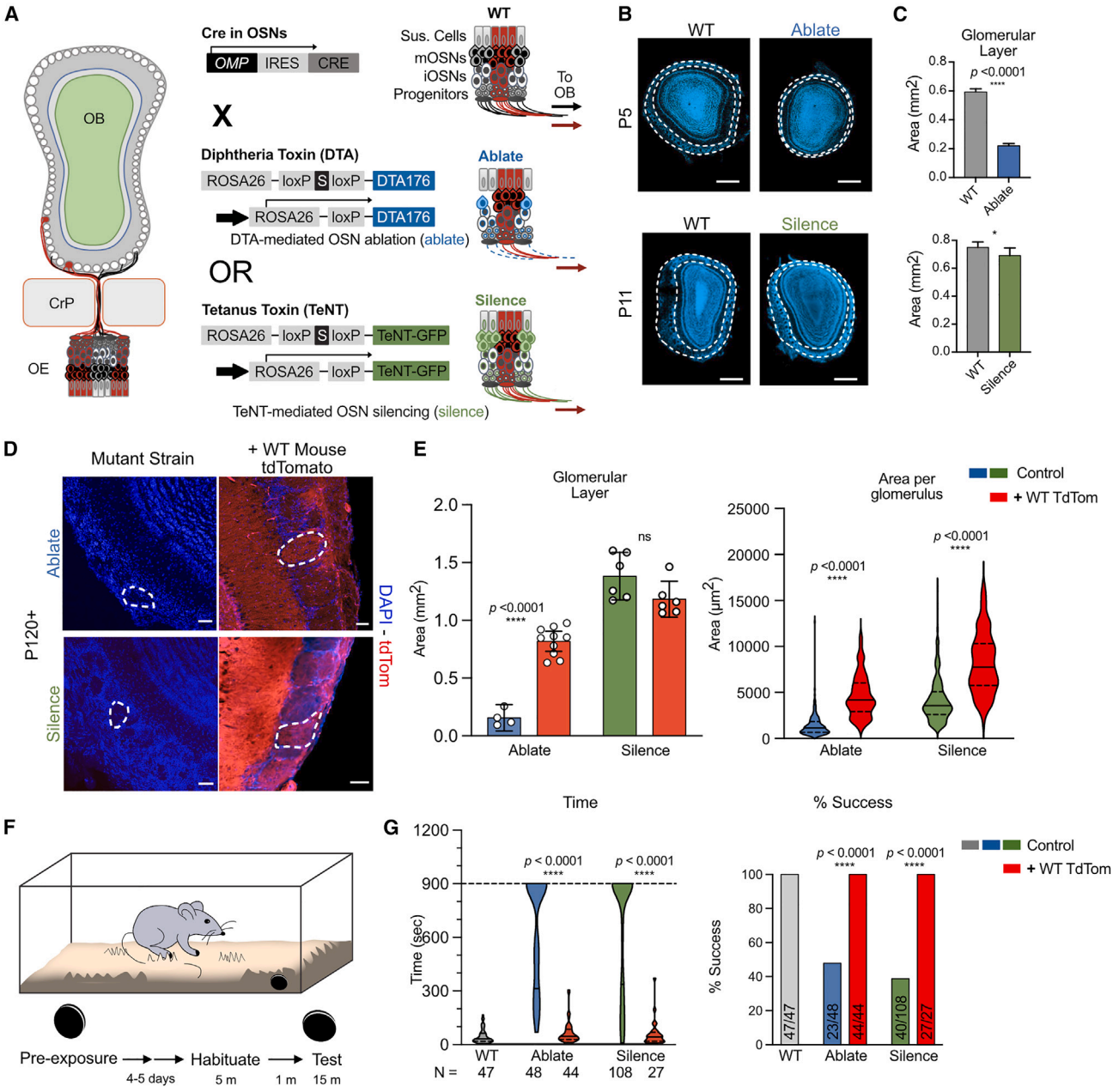

Figure 4. Genetic disability models and mouse-mouse olfactory complementation

(A) Schematic of genetic strategies: crossing OMP-Cre mice with floxed DTA and TeNT animals to Ablate (DTA) or Silence (TeNT) mouse OSNs.

(B) Olfactory bulb (OB) from wild-type (WT) and Ablate mice at P5 (top) and OBs in WT vs. Silence P11 (bottom) (nuclei in blue, DAPI). Dotted lines encircle the glomerular layer. Scale bars, 500 μm.

(C) Glomerular layer size is reduced in both models. Data are mean ± 95% CI; WT $n = 9$; Silence, $n = 6$ (top); WT, $n = 15$; and Ablate, $n = 11$ (bottom). Significance tested by two-tailed, unpaired t test, $^{*}p < 0.05$, $^{****}p < 0.0001$.

(D) Red mouse PSCs expressing tdTomato rescue OB deficits in both models. Ablate and Silence mutant strains (left) and mouse (tdTomato WT) chimeric rescue (right); DAPI (blue) and tdTomato (red). Scale bars, 50 μm.

(E) Glomerular layer size (bar graph, left) and individual glomerulus size (violin plot, right). For glomerular layer, data shown are means ± 95% CI; Silence (control), $n = 6$ and +WT TdTom, $n = 6$; Ablate (control), $n = 4$ and +WT TdTom, $n = 10$. *p values* shown are two-tailed unpaired t test. $^{****}p < 0.0001$. For individual glomerular size, violin plots with the median, upper, and lower quartiles are plotted; Silence(control), $n = 260$ glomeruli and +WT TdTom, $n = 134$ glomeruli; Ablate (control), $n = 141$ glomeruli and +WT TdTom, $n = 260$ glomeruli. Significance was tested by two-tailed unpaired t test, $^{****}p < 0.0001$.

(F) Schematic of the buried cookie (round black and white object) test.

(legend continued on next page)

Rat chimeras contribute to mouse olfactory sensory circuits

These results raise two central questions. Can rat neurons contribute to the olfactory sensory epithelium? And how well can they complement it in cases of loss or silencing of the neurons? Immunostaining of WT rat-mouse chimeras shows that rat OSNs populate the OE and express OMP, a key marker of maturity. Moreover, they extend axons into the OB that can persist for up to 2 years (Figures S5A and S5B). Electron microscopy shows that rat and mouse neurons can form synaptic structures in the OB synapses by staining for KsO (only in the rat cells) and performing immunogold labeling (Figures 5B, S5B, and S5C).

Which genome might govern the formation of the olfactory sensory map in interspecies chimeras? In the intraspecies mouse-mouse glomeruli, donor red fibers intermix with the unlabeled host mouse axons (Figure 4D). In contrast, in mice genetically engineered to express a rat OR in place of a mouse receptor, mouse OSNs with the rat OR form unique glomeruli.[25,26] In this case, the rat genome seems to drive circuit formation since rat-mouse OBs have distinct rat and mouse glomeruli without substantive mixed innervation (Figures 5C and S5D). If this is the case, we would expect that (1) all or most of the mouse OSN types and their corresponding glomeruli would be present; (2) any rat glomeruli could then constitute additional glomeruli, raising the total number of glomeruli present; and (3) the rat glomeruli could have overlapping or non-overlapping response properties to the mouse. We counted the numbers of glomeruli from serial OB sections of young animals with rat OSN contribution to only one OB hemisphere (Figure 5C). OBs with rat glomeruli had a small but significant increase in the number of glomeruli, compared with OBs lacking rat OSN innervation, further suggesting that rat OSNs form additional independent glomeruli in the mouse OB (Figure 5C). Overall, these results indicate that rat neurons can alter their birth dates and precise patterns (and lengths) of axonal projections based on cues in the mouse, yet they still build their own unique sensory processing structures, likely based on evolutionarily distinct gene sequences in their genome.

Anatomic and functional complementation in primary rat-mouse neural circuits

Since anatomic studies of rat OSNs in chimeras suggest the possibility of functional rescue, we wished to systematically test their capacity to rescue successive levels of specific olfactory circuit anatomy and function, using the Ablate and Silence models (Table 1; Figure 5D). In the OE, rat cells contribute to nearly all cells in the Ablate model, as expected, since the mouse OSNs are missing (Figure 5E). In the Silence model rat neurons intermix with mouse cognate (but silent) neurons (Figure 5E). The stem cells that produce OSNs also produce the supporting sustentacular cells, and this can be seen in OE sections as "columns," yet in other sections some OSNs migrate out forming distinct cell layers (Figures 5E and 5F), as has been reported in same-species complementation.[29] This indicates that rat cells can contribute to the basal stem cell population that produces OSNs throughout the life of the animal and concurs with the persistence of red rat glomeruli in aged mice (Figure S5A).

In the WT OB, rat glomeruli were significantly smaller than those found in WT mice (Figures 6A, 5B, and S5D). In contrast, Silence OBs exhibited robust innervation of glomeruli and a largely normal glomerular area, while in the Ablate OBs the rat glomeruli were similar to the mouse since most were very small (Figures 5A, 5B, and S5D). However, in certain local regions we could identify rat rescue at the level of glomerular structure (Figures 6A and S6A). These results show that despite their millions of years of evolutionary distance and their distinct differences in OB size and complexity, the rat OSNs maintain sufficient plasticity to innervate and partly rescue the structure of the OE to OB circuit.

Are rat OSNs communicating with the local circuits in the OB? In the OB, inhibitory periglomerular neurons directly surrounding glomeruli receive direct input from OSNs and express tyrosine hydroxylase (TH) in a synaptic activity-dependent manner.[33] Rat-driven TH expression was slightly decreased in the WT mice and strongly rescued in the Silence model (Figures 6A and 6C). In the Ablate model, the overall amount of TH was not significantly rescued across the entire OB, but we can detect local areas where the glomeruli are larger with increased TH expression (Figures 6A and 6C). The increase in TH suggests that active rat glomeruli may be "winners" in the known activity-dependent competition between glomeruli in the OB (Figures 6A–6C).

Cortical processing and olfactory behavior in distinct rat complementation models

Rat OSNs can drive activity-dependent gene expression in the OB. However, the next stage of olfactory processing requires that OSNs form synapses with MT neurons, then correctly signal to the target neurons in the cortex. Rat OSNs might have innate differences in their synaptic strength, timing of vesicle release, or other characteristics that disrupt interspecies information transfer. To test this, we took advantage of the fact that olfactory information is transmitted to the cortex only ipsilaterally and not contralaterally.[34–41] In both our Ablate and Silence models, and in WT mice, we identified chimeras with unilateral rat contribution to OSNs in the OE and OB by visual inspection of the brains at dissection and subsequent confirmation by taking serial sections through the entire OB (Figure S6B). We reasoned that we could determine whether rat neurons can communicate to the mouse olfactory cortex by directly comparing the silent "mouse-only" cortical hemisphere with the potentially rescued "rat-mouse" hemisphere, using serial sections taken from the same animal's

(G) WT Mouse PSCs rescue behavior in both models. For time, violin plots with the median and the upper and lower quartile are shown. WT, $n = 47$. Ablate (non-chimera), $n = 7$; Ablate (+WT TdTom), $n = 44$. Silence (non-chimera), $n = 27$; Silence (+WT TdTom), $n = 27$. Significance was tested by repeated measures one-way ANOVA with Dunn's multiple comparisons test. For percent success, the test was deemed successful if the cookie was found under 900 s. For the Ablate non-chimeras, 5/7 were successful while 44/44 were rescued by WT mouse chimerism. For the Silence model, 27/27 non-chimeras were successful. Significance tested by Fisher's exact test.
See also Figure S4.

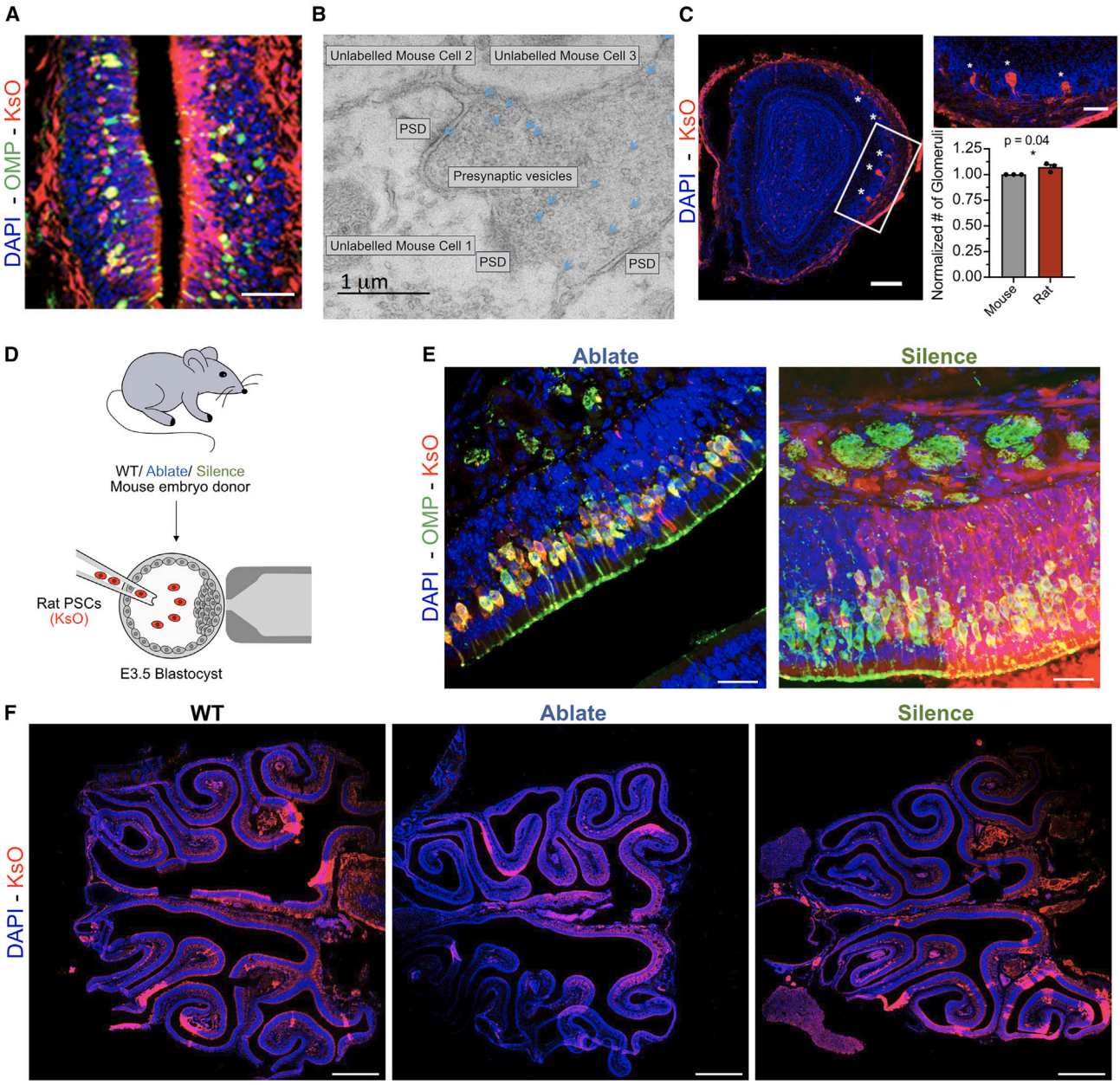

Figure 5. Rat-mouse anatomic complementation

(A) OMP-positive rat OSNs in a rat-mouse chimera, nuclei (DAPI, blue), OMP (green), and rat KsO (red). Scale bars, 100 μm.

(B) Transmission electron microscopy on rat-mouse chimeric synapses labeled with immunogold staining against KsO as indicated by dark densities marked by blue arrows. Synapses between rat and mouse cells with presynaptic vesicles and postsynaptic densities (PSD) labeled.

(C) OB section shows glomeruli with majority rat cells or no rat cells in a P10 rat-mouse chimera; rat KsO (red) and nuclei (DAPI, blue). Asterisks mark rat glomeruli. White box is inset. Scale bars, 250 and 100 μm (inset). Total number of glomeruli in animals with unilateral rat OSN contribution (right), normalized to the hemisphere without rat glomeruli. Mean ± 95% CI, $n = 3$ animals, 32 slices/animal. Significance tested by a two-tailed unpaired t test, $^{*}p = 0.0412$.

(D) Schematic of rat PSCs expressing KsO injected into mouse embryos.

(E) Olfactory epithelium (OE) in chimeric rat rescue of Ablate (left) or Silence (right) mouse blastocyst; nuclei (DAPI, blue), rat (KsO, red), and OMP (green). Scale bars, 25 μm.

(F) OE from rat mouse chimeras in labeled mouse background; nuclei (DAPI, blue) and rat (KsO, red). Scale bars, 500 μm.

See also Figure S5.

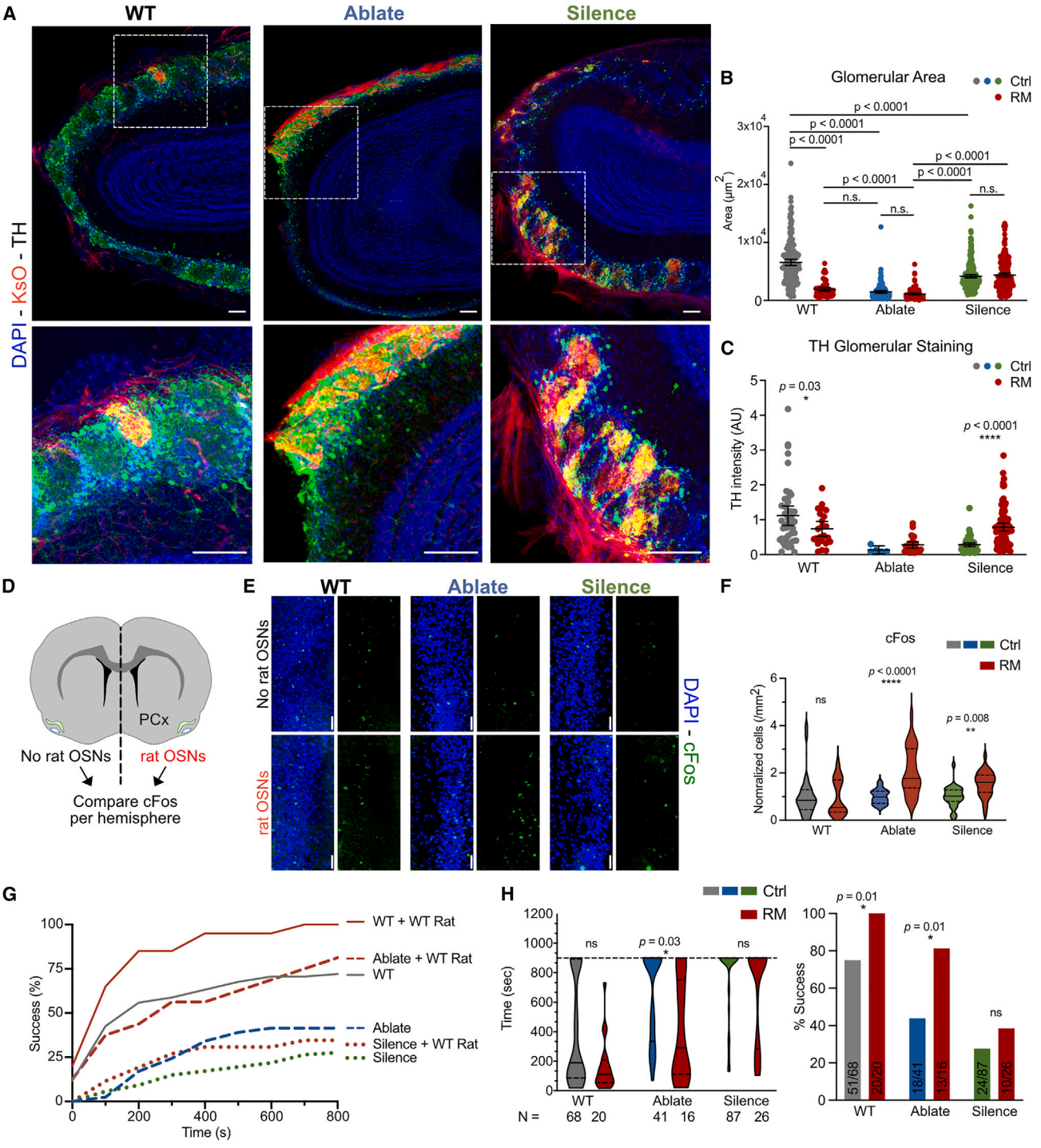

Figure 6. Rat neurons rescue synaptic communication and behavior in anosmic mice

(A) Rat and mouse glomeruli stained for tyrosine hydroxylase (TH, green), nuclei (DAPI, blue), and rat KsO (red). Scale bars, 100 μm.

(B) Glomerulus size across models. Scatterplots with mean ± 95% CI; n = 3–4 animals/genotype, 2–3 slices/animal, 191 glomeruli (WT-mouse), 68 (WT mouse-rat chimera), 141 (Ablate-mouse), 145 (Ablate mouse-rat chimera), 260 (Silence-mouse), and 232 (Silence mouse-rat chimera). Significance tested by 2-way ANOVA followed by Tukey's multiple comparisons test. ****$p < 0.0001$, **$p < 0.01$.

(C) Rat OSNs rescue TH only in the Silence model. Scatterplots with mean ± 95% CI; n = 1 animal/genotype, 3 slices/animal, 44 glomeruli (WT-mouse), 23 (WT mouse-rat chimera), 5 (Ablate-mouse), 25 (Ablate mouse-rat chimera), 60 (Silence-mouse), and 95 (Silence mouse-rat chimera). Significance by two-way ANOVA and Sídák's multiple comparisons test. *$p < 0.0248$, ****$p < 0.0001$.

(legend continued on next page)

brain (Figures 6D and 6E). This sensitive and rigorous design is important because the chimeras have stochastic contribution to OSNs, such that different chimeras are likely to have different OR repertoires and also different olfactory environments. Measuring baseline activity in two hemispheres of the same brain across the same anterior-posterior (A-P) axis in a complex odor environment should control for these differences.

Here, we analyze the PCx, which is responsible for odor perception and discrimination.[34–41] Loss or silencing of OSNs, achieved by multiple methods, has been shown to reduce activity and immediate early gene (IEG) expression in the PCx, while OSN sensory activity reliably increases c-Fos expression in the (PCx).[34–41] Therefore, the use of c-Fos to detect odor-evoked OSN activity transferred through MT neurons to the PCx is well established as a readout of OSN activity.[38] We first showed that we detect less c-Fos in the PCx of non-chimeric Ablate and Silence mice than in WT mice (Figure S6C). We next examined c-Fos expression in the PCx of chimeras with unilateral rat OSN contribution in WT, Ablate, and Silence mouse models. Rat OSN contribution significantly increased c-Fos expression in the ipsilateral PCx of both Ablate and Silence chimeras, compared with the same animal contralateral sections (Figures 6D–6F). This increase was not seen in WT chimeras, as expected. Thus, these data demonstrate that sensory information flow derived from peripheral rat sensory neurons can be communicated to the PCx at the sensitivity level of c-Fos induction. Unexpectedly, the rescue in the Ablate model was greater than in the Silence model, even though the IEG (TH) activity in the local OB circuit showed the reverse pattern. One explanation for this could be that rat OSN signals are relatively stronger in the Ablate PCx due to less local inhibition or less competition with resident mouse OSNs, but other explanations are possible.

Behavioral rescue

Finally, we wished to test whether rat OSNs could rescue the sense of smell in the anosmic mouse models. We again employed the buried cookie test. Unexpectedly, rat OSNs rescued food-seeking behavior in the Ablate but not in the Silence models (Figures 6G and 6H). This is consistent with the more robust increase in c-Fos staining in the cortex of Ablate rat chimeras than in the Silence models. However, the rescue was not as robust as in the mouse-mouse experiments shown in Figure 4. WT mouse olfaction appeared slightly improved in rat-mouse chimeras when measuring percent success but not time to find the cookie. The improved rescue capability of rat neurons in the Ablate animals was not expected, but it may indicate that competition from the Silence mouse OSNs can interfere with rat sensory signals to cortical circuits, although other explanations are also possible.

DISCUSSION

We show that rat PSCs can develop within a mouse embryo to produce a chimeric brain with functional neural circuits built from neurons of two species. Despite development in an evolutionarily divergent host, rat cells readily differentiate into diverse morphological neuronal subtypes that populate nearly all brain regions. Rat neurons form layered cortical structures synchronously with the host mouse cells. They also establish dynamic synaptic structures such as OB glomeruli that persist for nearly two years. Activity mapping studies show that they can engage in multilevel interspecies synaptic communication from the periphery to the mouse cortex. Finally, rat neurons pass the gold standard test of function, by driving a specific behavior using the appropriate cognate neurons to wire into specific mouse neural circuits.

Interestingly, despite this remarkable interspecies plasticity, we find that certain rat-specific programs override mouse developmental control. For example, rat neurons form rat-dominant glomeruli that may afford mice improved or even novel sensory sensitivities due to the different molecular receptive fields of their divergent ORs or simply a larger set of ORs for combinatorial odor encoding. In other contexts, rat neurons fail to rescue important cues from the mouse brain; for example, they cannot fully rescue local OB structures when mouse OSNs are missing.

Although we show that rat cells can partly rescue the primal mouse olfactory behavior of food seeking, this only succeeds when mouse cells are absent but not when mouse cells are silenced. In contrast, same-species complementation is more robust than rat-mouse rescue and works in both Ablate and Silence models. This disparity might be explained somewhat trivially by the generally lower contribution of rat cells, compared with mouse cells, in complementation studies. Alternatively, or in addition, there may be species-specific blockades to behavioral rescue. These could include differences in the molecules that drive the finer details of synaptic connectivity, set neuronal firing rates, or regulate intrinsic properties (such as excitability) that may have evolved differently across species with different-sized brains. In support of this idea, mouse and rat proteins differ by about 4% at the amino acid level (93.6% conservation).[42] This percent divergence can have clear consequences for circuit formation. For example, the OR I7 is 95% conserved between rat and mouse and

(D) A schematic illustrating unilateral rat contribution internal comparison for c-Fos in the piriform cortex (PCx).
(E) c-Fos staining in left and right hemisphere PCx of animals with unilateral rat OSNs; nuclei (DAPI, blue) and c-Fos (green). Scale bars, 50 μm.
(F) Rat OSN contribution increases c-Fos expression in the ipsilateral PCx. Cell densities were normalized to the mean density in the no contribution hemisphere for each animal. Violin plots with the median and upper and lower quartiles are shown; $n = 2$ animal/genotype, 15 slices/animal. Significance tested by two-way ANOVA followed by Sídák's multiple comparisons test, $^{**}p < 0.01$, $^{****}p < 0.0001$.
(G) WT rat PSCs rescue behavior in the Ablate model. Cumulative cookie-finding success of chimeras per second (s).
(H) (Left) Rat contribution rescues time to find the cookie in Ablate models, shown as violin plots with median and the upper and lower quartile. WT, n =68; WT (rat-mouse chimeras), $n = 20$; Ablate (control), $n = 41$; Ablate (rat-mouse chimeras), $n = 16$; Silence (control), $n = 87$, Silence (rat-mouse chimeras), $n = 26$. Significance tested by repeated measures one-way ANOVA with Dunn's multiple comparisons test (left panel). Significance was tested by Fisher's exact test, $^{*}p < 0.05$ with exact p values listed (right panel).
See also Figure S6.

responds to similar odor ligands.[43] Yet, transgenic expression of rat OR I7 in mouse OSNs leads to formation of an independent rat glomerulus that does not mix with the mouse.[44] Related to this, a strength of interspecies blastocyst chimeras over transplant models is that it allows rat neurons to transit through all stages of embryonic and brain development concomitantly with the mouse. This exposes the rat cells to multiple levels of cell-cell competition, in which they might fail to wire correctly. Interspecies brain chimeras, therefore, offer a powerful tool to explore the molecular basis for these barriers.

Cre lines and other conditional expression systems such as doxycycline-inducible activators and viral transduction have been used to examine the roles of small numbers of genes in an otherwise isogenic background. In contrast, the selective neural blastocyst complementation technique allows for testing of any genome of any species or strain for its capacity to form circuits and function in a living animal and throughout its lifetime. Examples of capabilities made possible by this work are as follows: (1) testing widely divergent mouse strains with different propensities for disease; (2) modeling human traits that are polygenic, by combining many heterozygous mutations in a single PSC through genome editing; and (3) testing the limits of brain plasticity and the constraints of evolution, by generating chimeras from species with different sensory capacities or lifespans. Finally, these systems may also be used to examine cell-autonomous sex differences by putting female neurons into male brains and the reverse. These studies also can be useful in designing and interpreting larger-scale region-specific interspecies cell replacements, as described in the related paper in this issue.[45]

Limitations of the study

These studies are meant to provide proof of principle that rat-mouse chimeric brains can form interspecies neural circuits of varying function, setting the stage for future uses of these systems. While we did not directly demonstrate that the fluorescent red KsO neurons or the ''yellow'' YFP neurons in an intact mouse chimera brain were from rat, using independent immunostaining of rat-specific proteins, our lab cultured and derived these lines from rat cells maintained in rat media, and we observed functional differences *in situ* between mouse and rat cells including the formation of rat-specific glomeruli (KsO cells) and the selective activation via light with the rat ChR2-eYFP chimeras. We also showed that both rat and mouse neuronal genes are expressed in chimeric brains and confirmed the species of origin of all PSC lines with PCR.

A second limitation common to all blastocyst complementation studies is the stochastic contribution of the donor rat neurons to different circuits in different mice. This practically prohibits many studies that we would find intriguing, such as examining more behaviors or dissecting out contributions to other sensory systems or neural circuits by using different Cre lines. However, in some cases the stochastic and asymmetric donor cell contribution may be harnessed to the investigator's advantage, as in our examination of odor-evoked activity in the cortex of individual mice with rat neurons in only one hemisphere.

In this study, we focused on the major unknown question of whether residence in a mouse brain and evidence of synaptic connectivity are equivalent to meaningful neural communication. We tested this using the primal odor-guided behavior of food seeking. Given the diversity of rat contribution to various neuronal populations, this required us to use most of our candidate chimeras for this specific untrained behavioral test (~900 rat-mouse chimeras over >4 years, across two locations) to achieve the necessary statistical power. While this currently remains an inherent limitation to the system, we anticipate that new genetic methods to guide or restrict donor cell fate may soon overcome these obstacles.

STAR★METHODS

Detailed methods are provided in the online version of this paper and include the following:

- KEY RESOURCES TABLE
- RESOURCE AVAILABILITY
  - Lead contact
  - Materials availability
  - Data and code availability
- EXPERIMENTAL MODEL AND STUDY PARTICIPANT DETAILS
  - Mouse strains
  - Cell culture conditions
- METHOD DETAILS
  - Generation of chimeras
  - Tissue preparation and immunostaining
  - Nucleic acid extraction and PCR
  - Lentiviral constructs and production
  - Rat iPSC reprogramming
  - Lentiviral-integrated iPSC subclones
  - Animal behavior assay
  - Acute slice electrophysiology, recording, and analysis
  - Dual-pulse birth dating, staining, and analysis
  - Transmission Electron Microscopy
  - Whole-brain image acquisition
- QUANTIFICATION AND STATISTICAL ANALYSIS
  - Confocal imaging, image processing, and analysis
  - ROI Brain Area Analysis
  - Whole-brain registration
  - Brain Signal Segmentation
  - Statistical Analyses

ACKNOWLEDGMENTS

The authors thank Kathryn Spencer for microscopy assistance, Valentina Lo Sardo and Steffany Dunn for help with iPSC reprogramming and subcloning, Ling Li for preparing brain sections, Anastasia Bludova for light-sheet brain imaging, and Sammy Weiser Novak and Leonardo R. Andrade of the Waitt Advanced Biophotonics Center at the Salk Institute for Biological Studies for electron microscopy. We thank Dr. Qi-long Ying for providing DAC2 and DAC8 rat ESCs. J.W. is a an NYSCF-Robertson Investigator and Virginia Murchison Linthicum Scholar in Medical Research. Support was provided as follows: to J.C.I.B., G. Harold and Leila Y. Mathers Charitable Foundation, The Moxie Foundation, The Leona M. and Harry B. Helmsley Charitable Trust (2012-PG-MED002), The Hewitt Foundation, NIH (5 DP1 DK113616), and Universidad Católica San Antonio de Murcia; to J.W., Cancer Prevention &

Research Institute of Texas (#RR170076), NYSCF, NIH (HD103627-01A1), and The Welch Foundation (I-2088); to K.K.B., RF1AG079517, R56AG062618, DP1AG055944, R01 MH102698, and R01 DC012592; and to M.K.b.I., Swiss National Science Foundation. A.L.H. was supported by a fellowship from the American Epilepsy Society (5–79096).

AUTHOR CONTRIBUTIONS

Conceptualization, K.K.B., J.W., J.C.I.B., and B.T.T; methodology and investigation, B.T.T., M.K.b.I, R.M.-C., M.S., A.L.H., K.N.J., A.R.R., G.M., and Z.W.; formal analysis, R.M.-C.; writing – original draft, B.T.T., K.K.B., J.W., M.K.b.I., and R.M.-C.; writing – review & editing, S.K., J.W., J.C.I.B., B.T.T., M.K.b.I., and K.K.B.; visualization, B.T.T., K.K.B., J.W., M.K.b.I., and R.M.-C.; resources, K.N.J. and J.C.I.B.; supervision, G.L., S.K., Z.W., P.O., J.W., J.C.I.B., and K.K.B.; funding acquisition, K.K.B., J.W., and J.C.I.B.

DECLARATION OF INTERESTS

K.K.B. is on the SAB of Gameto Therapeutics. B.T.T. is a current employee of Janssen Research and Development. P.O. is a founder of Theracast. J.C.I.B is a founding scientist and director of the San Diego Institute of Science, Altos Labs.

Received: May 5, 2023
Revised: January 18, 2024
Accepted: March 26, 2024
Published: April 25, 2024

REFERENCES

1. Isotani, A., Hatayama, H., Kaseda, K., Ikawa, M., and Okabe, M. (2011). Formation of a thymus from rat ES cells in xenogeneic nude mouse↔rat ES chimeras. Genes Cells *16*, 397–405. https://doi.org/10.1111/j.1365-2443.2011.01495.x.
2. Isotani, A., Yamagata, K., Okabe, M., and Ikawa, M. (2016). Generation of Hprt-disrupted rat through mouse←rat ES chimeras. Sci. Rep. *6*, 24215. https://doi.org/10.1038/srep24215.
3. Wu, J., Platero-Luengo, A., Sakurai, M., Sugawara, A., Gil, M.A., Yamauchi, T., Suzuki, K., Bogliotti, Y.S., Cuello, C., Morales Valencia, M., et al. (2017). Interspecies Chimerism with Mammalian Pluripotent Stem Cells. Cell *168*, 473–486.e15. https://doi.org/10.1016/j.cell.2016.12.036.
4. Xiang, A.P., Mao, F.F., Li, W.Q., Park, D., Ma, B.F., Wang, T., Vallender, T.W., Vallender, E.J., Zhang, L., Lee, J., et al. (2008). Extensive contribution of embryonic stem cells to the development of an evolutionarily divergent host. Hum. Mol. Genet. *17*, 27–37. https://doi.org/10.1093/hmg/ddm282.
5. Yamaguchi, T., Sato, H., Kato-Itoh, M., Goto, T., Hara, H., Sanbo, M., Mizuno, N., Kobayashi, T., Yanagida, A., Umino, A., et al. (2017). Interspecies organogenesis generates autologous functional islets. Nature *542*, 191–196. https://doi.org/10.1038/nature21070.
6. Chen, J., Lansford, R., Stewart, V., Young, F., and Alt, F.W. (1993). RAG-2-deficient blastocyst complementation: an assay of gene function in lymphocyte development. Proc. Natl. Acad. Sci. USA *90*, 4528–4532. https://doi.org/10.1073/pnas.90.10.4528.
7. Kobayashi, T., Yamaguchi, T., Hamanaka, S., Kato-Itoh, M., Yamazaki, Y., Ibata, M., Sato, H., Lee, Y.S., Usui, J., Knisely, A.S., et al. (2010). Generation of Rat Pancreas in Mouse by Interspecific Blastocyst Injection of Pluripotent Stem Cells. Cell *142*, 787–799. https://doi.org/10.1016/j.cell.2010.07.039.
8. Usui, J., Kobayashi, T., Yamaguchi, T., Knisely, A.S., Nishinakamura, R., and Nakauchi, H. (2012). Generation of Kidney from Pluripotent Stem Cells via Blastocyst Complementation. Am. J. Pathol. *180*, 2417–2426. https://doi.org/10.1016/j.cell.2010.07.039.
9. Mori, M., Furuhashi, K., Danielsson, J.A., Hirata, Y., Kakiuchi, M., Lin, C.S., Ohta, M., Riccio, P., Takahashi, Y., Xu, X., et al. (2019). Generation of functional lungs via conditional blastocyst complementation using pluripotent stem cells. Nat. Med. *25*, 1691–1698. https://doi.org/10.1038/s41591-019-0635-8.
10. Goto, T., Hara, H., Sanbo, M., Masaki, H., Sato, H., Yamaguchi, T., Hochi, S., Kobayashi, T., Nakauchi, H., and Hirabayashi, M. (2019). Generation of pluripotent stem cell-derived mouse kidneys in Sall1-targeted anephric rats. Nat. Commun. *10*, 451. https://doi.org/10.1038/s41467-019-08394-9.
11. Chang, A.N., Liang, Z., Dai, H.Q., Chapdelaine-Williams, A.M., Andrews, N., Bronson, R.T., Schwer, B., and Alt, F.W. (2018). Neural blastocyst complementation enables mouse forebrain organogenesis. Nature *563*, 126–130. https://doi.org/10.1038/s41586-018-0586-0.
12. Li, P., Tong, C., Mehrian-Shai, R., Jia, L., Wu, N., Yan, Y., Maxson, R.E., Schulze, E.N., Song, H., Hsieh, C.L., et al. (2008). Germline Competent Embryonic Stem Cells Derived from Rat Blastocysts. Cell *135*, 1299–1310. https://doi.org/10.1016/j.cell.2008.12.006.
13. Semple, B.D., Blomgren, K., Gimlin, K., Ferriero, D.M., and Noble-Haeusslein, L.J. (2013). Brain development in rodents and humans: Identifying benchmarks of maturation and vulnerability to injury across species. Prog. Neurobiol. *106–107*, 1–16. https://doi.org/10.1016/j.pneurobio.2013.04.001.
14. Espuny-Camacho, I., Michelsen, K.A., Gall, D., Linaro, D., Hasche, A., Bonnefont, J., Bali, C., Orduz, D., Bilheu, A., Herpoel, A., et al. (2013). Pyramidal neurons derived from human pluripotent stem cells integrate efficiently into mouse brain circuits in vivo. Neuron *77*, 440–456. https://doi.org/10.1016/j.neuron.2012.12.011.
15. Falkner, S., Grade, S., Dimou, L., Conzelmann, K.K., Bonhoeffer, T., Götz, M., and Hübener, M. (2016). Transplanted embryonic neurons integrate into adult neocortical circuits. Nature *539*, 248–253. https://doi.org/10.1038/nature20113.
16. Espuny-Camacho, I., Michelsen, K.A., Linaro, D., Bilheu, A., Acosta-Verdugo, S., Herpoel, A., Giugliano, M., Gaillard, A., and Vanderhaeghen, P. (2018). Human Pluripotent Stem-Cell-Derived Cortical Neurons Integrate Functionally into the Lesioned Adult Murine Visual Cortex in an Area-Specific Way. Cell Rep. *23*, 2732–2743. https://doi.org/10.1016/j.celrep.2018.04.094.
17. Linaro, D., Vermaercke, B., Iwata, R., Ramaswamy, A., Libé-Philippot, B., Boubakar, L., Davis, B.A., Wierda, K., Davie, K., Poovathingal, S., et al. (2019). Xenotransplanted Human Cortical Neurons Reveal Species-Specific Development and Functional Integration into Mouse Visual Circuits. Neuron *104*, 972–986.e6. https://doi.org/10.1016/j.neuron.2019.10.002.
18. Oberst, P., Fièvre, S., Baumann, N., Concetti, C., Bartolini, G., and Jabaudon, D. (2019). Temporal plasticity of apical progenitors in the developing mouse neocortex. Nature *573*, 370–374. https://doi.org/10.1038/s41586-019-1515-6.
19. Greig, L.C., Woodworth, M.B., Galazo, M.J., Padmanabhan, H., and Macklis, J.D. (2013). Molecular logic of neocortical projection neuron specification, development and diversity. Nat. Rev. Neurosci. *14*, 755–769. https://doi.org/10.1038/nrn3586.
20. Molyneaux, B.J., Arlotta, P., Menezes, J.R.L., and Macklis, J.D. (2007). Neuronal subtype specification in the cerebral cortex. Nat. Rev. Neurosci. *8*, 427–437. https://doi.org/10.1038/nrn2151.
21. Francis, C., Natarajan, S., Lee, M.T., Khaladkar, M., Buckley, P.T., Sul, J.Y., Eberwine, J., and Kim, J. (2014). Divergence of RNA localization between rat and mouse neurons reveals the potential for rapid brain evolution. BMC Genomics *15*, 883. https://doi.org/10.1186/1471-2164-15-883.
22. Zhang, F., Wang, L.P., Brauner, M., Liewald, J.F., Kay, K., Watzke, N., Wood, P.G., Bamberg, E., Nagel, G., Gottschalk, A., et al. (2007). Multimodal fast optical interrogation of neural circuitry. Nature *446*, 633–639. https://doi.org/10.1038/nature05744.
23. Young, J.M., Friedman, C., Williams, E.M., Ross, J.A., Tonnes-Priddy, L., and Trask, B.J. (2002). Different evolutionary processes shaped the mouse and human olfactory receptor gene families. Hum. Mol. Genet. *11*, 535–546. https://doi.org/10.1093/hmg/11.5.535.

24. Zhang, X., and Firestein, S. (2002). The olfactory receptor gene superfamily of the mouse. Nat. Neurosci. *5*, 124–133. https://doi.org/10.1038/nn800.

25. Belluscio, L., Lodovichi, C., Feinstein, P., Mombaerts, P., and Katz, L.C. (2002). Odorant receptors instruct functional circuitry in the mouse olfactory bulb. Nature *419*, 296–300. https://doi.org/10.1038/nature01001.

26. Bozza, T., Feinstein, P., Zheng, C., and Mombaerts, P. (2002). Odorant Receptor Expression Defines Functional Units in the Mouse Olfactory System. J. Neurosci. *22*, 3033–3043. https://doi.org/10.1523/jneurosci.22-08-03033.2002.

27. Gogos, J.A., Osborne, J., Nemes, A., Mendelsohn, M., and Axel, R. (2000). Genetic Ablation and Restoration of the Olfactory Topographic Map. Cell *103*, 609–620. https://doi.org/10.1016/s0092-8674(00)00164-1.

28. Zhang, X., Zhang, X., and Firestein, S. (2007). Comparative Genomics of Odorant- and Pheromone Receptor Genes in Rodents. Genomics *89*, 441–450. https://doi.org/10.1016/j.ygeno.2007.01.002.

29. Eggan, K., Baldwin, K., Tackett, M., Osborne, J., Gogos, J., Chess, A., Axel, R., and Jaenisch, R. (2004). Mice cloned from olfactory sensory neurons. Nature *428*, 44–49. https://doi.org/10.1038/nature02375.

30. Yu, C.R., Power, J., Barnea, G., O'Donnell, S., Brown, H.E., Osborne, J., Axel, R., and Gogos, J.A. (2004). Spontaneous Neural Activity Is Required for the Establishment and Maintenance of the Olfactory Sensory Map. Neuron *42*, 553–566. https://doi.org/10.1016/s0896-6273(04)00224-7.

31. James, K.N., Throesch, B.T., Davini, W., Eade, K.T., Ghosh, S., Lee, S., Torabi-Rander, N., and Baldwin, K.K. (2017). Activity based checkpoints ensure circuit stability in the olfactory system. Preprint at bioRxiv. https://doi.org/10.1101/156372.

32. Machado, C.F., Reis-Silva, T.M., Lyra, C.S., Felicio, L.F., and Malnic, B. (2018). Buried Food-seeking Test for the Assessment of Olfactory Detection in Mice. Bio Protoc. *8*, e2897. https://doi.org/10.21769/BioProtoc.2897.

33. McLean, J.H., and Shipley, M.T. (1988). Postmitotic, postmigrational expression of tyrosine hydroxylase in olfactory bulb dopaminergic neurons. J. Neurosci. *8*, 3658–3669. https://doi.org/10.1523/jneurosci.08-10-03658.1988.

34. Schneider, S.P., and Scott, J.W. (1983). Orthodromic response properties of rat olfactory bulb mitral and tufted cells correlate with their projection patterns. J. Neurophysiol. *50*, 358–378. https://doi.org/10.1152/jn.1983.50.2.358.

35. Scott, J.W. (1981). Electrophysiological identification of mitral and tufted cells and distributions of their axons in olfactory system of the rat. J. Neurophysiol. *46*, 918–931. https://doi.org/10.1152/jn.1981.46.5.918.

36. Franks, K.M., and Isaacson, J.S. (2005). Synapse-Specific Downregulation of NMDA Receptors by Early Experience: A Critical Period for Plasticity of Sensory Input to Olfactory Cortex. Neuron *47*, 101–114. https://doi.org/10.1016/j.neuron.2005.05.024.

37. Kim, H.H., Puche, A.C., and Margolis, F.L. (2006). Odorant Deprivation Reversibly Modulates Transsynaptic Changes in the NR2B-Mediated CREB Pathway in Mouse Piriform Cortex. J. Neurosci. *26*, 9548–9559. https://doi.org/10.1523/jneurosci.1727-06.2006.

38. Stettler, D.D., and Axel, R. (2009). Representations of odor in the piriform cortex. Neuron *63*, 854–864. https://doi.org/10.1016/j.neuron.2009.09.005.

39. Slattery, D.A., Morrow, J.A., Hudson, A.L., Hill, D.R., Nutt, D.J., and Henry, B. (2005). Comparison of Alterations in c-fos and Egr-1 (zif268) Expression Throughout the Rat Brain Following Acute Administration of Different Classes of Antidepressant Compounds. Neuropsychopharmacology *30*, 1278–1287. https://doi.org/10.1038/sj.npp.1300717.

40. Bepari, A.K., Watanabe, K., Yamaguchi, M., Tamamaki, N., and Takebayashi, H. (2012). Visualization of odor-induced neuronal activity by immediate early gene expression. BMC Neurosci. *13*, 140. https://doi.org/10.1186/1471-2202-13-140.

41. Dardou, D., Datiche, F., and Cattarelli, M. (2006). Fos and Egr1 expression in the rat brain in response to olfactory cue after taste-potentiated odor aversion retrieval. Learn. Mem. *13*, 150–160. https://doi.org/10.1101/lm.148706.

42. Wolfe, K.H., and Sharp, P.M. (1993). Mammalian gene evolution: Nucleotide sequence divergence between mouse and rat. J. Mol. Evol. *37*, 441–456. https://doi.org/10.1007/bf00178874.

43. Hall, S.E., Floriano, W.B., Vaidehi, N., and Goddard, W.A., III. (2004). Predicted 3-D Structures for Mouse I7 and Rat I7 Olfactory Receptors and Comparison of Predicted Odor Recognition Profiles with Experiment. Chem. Senses *29*, 595–616. https://doi.org/10.1093/chemse/bjh063.

44. Imai, T., Suzuki, M., and Sakano, H. (2006). Odorant receptor-derived cAMP signals direct axonal targeting. Science *314*, 657–661. https://doi.org/10.1126/science.1131794.

45. Huang, J., He, B., Yang, X., Long, X., Wei, Y., Li, L., Tang, M., Gao, Y., Fang, Y., Ying, W., et al. (2024). Generation of rat forebrain tissues in mice. Cell *187*, 2129–2142. https://doi.org/10.1016/j.cell.2024.03.017.

46. Dull, T., Zufferey, R., Kelly, M., Mandel, R.J., Nguyen, M., Trono, D., and Naldini, L. (1998). A third-generation lentivirus vector with a conditional packaging system. J. Virol. *72*, 8463–8471. https://doi.org/10.1128/jvi.72.11.8463-8471.1998.

47. Klein, S., Staring, M., Murphy, K., Viergever, M.A., and Pluim, J.P.W. (2010). Elastix: A toolbox for intensity-based medical image registration. IEEE Trans. Med. Imaging *29*, 196–205. https://doi.org/10.1109/tmi.2009.2035616.

48. Mattes, D., Haynor, D.R., Vesselle, H., Lewellen, T.K., and Eubank, W. (2003). PET-CT image registration in the chest using free-form deformations. IEEE Trans. Med. Imaging *22*, 120–128. https://doi.org/10.1109/tmi.2003.809072.

49. Zhang, Y., Narayan, S., Geiman, E., Lanuza, G.M., Velasquez, T., Shanks, B., Akay, T., Dyck, J., Pearson, K., Gosgnach, S., et al. (2008). V3 Spinal Neurons Establish a Robust and Balanced Locomotor Rhythm during Walking. Neuron *60*, 84–96. https://doi.org/10.1016/j.neuron.2008.09.027.

50. Voehringer, D., Liang, H.E., and Locksley, R.M. (2008). Homeostasis and effector function of lymphopenia-induced 'memory-like' T cells in constitutively T cell-depleted mice. J. Immunol. *180*, 4742–4753. https://doi.org/10.4049/jimmunol.180.7.4742.

51. Boland, M.J., Hazen, J.L., Nazor, K.L., Rodriguez, A.R., Gifford, W., Martin, G., Kupriyanov, S., and Baldwin, K.K. (2009). Adult mice generated from induced pluripotent stem cells. Nature *461*, 91–94. https://doi.org/10.1038/nature08310.

52. Hazen, J.L., Faust, G.G., Rodriguez, A.R., Ferguson, W.C., Shumilina, S., Clark, R.A., Boland, M.J., Martin, G., Chubukov, P., Tsunemoto, R.K., et al. (2016). The Complete Genome Sequences, Unique Mutational Spectra, and Developmental Potency of Adult Neurons Revealed by Cloning. Neuron *89*, 1223–1236. https://doi.org/10.1016/j.neuron.2016.02.004.

53. Go, W.Y., and Ho, S.N. (2002). Optimization and direct comparison of the dimerizer and reverse tet transcriptional control systems. J. Gene Med. *4*, 258–270. https://doi.org/10.1002/jgm.271.

54. Thompson, C.L., Ng, L., Menon, V., Martinez, S., Lee, C.K., Glattfelder, K., Sunkin, S.M., Henry, A., Lau, C., Dang, C., et al. (2014). A High-Resolution Spatiotemporal Atlas of Gene Expression of the Developing Mouse Brain. Neuron *83*, 309–323. https://doi.org/10.1016/j.neuron.2014.05.033.

55. Graham, F.L., and van der Eb, A.J. (1973). A new technique for the assay of infectivity of human adenovirus 5 DNA. Virology *52*, 456–467. https://doi.org/10.1016/0042-6822(73)90341-3.

56. Pologruto, T.A., Sabatini, B.L., and Svoboda, K. (2003). ScanImage: Flexible software for operating laser scanning microscopes. Biomed. Eng. Online *2*, 13. https://doi.org/10.1186/1475-925x-2-13.

57. Schindelin, J., Arganda-Carreras, I., Frise, E., Kaynig, V., Longair, M., Pietzsch, T., Preibisch, S., Rueden, C., Saalfeld, S., Schmid, B., et al. (2012). Fiji: an open-source platform for biological-image analysis. Nat. Methods *9*, 676–682. https://doi.org/10.1038/nmeth.2019.

58. Kim, Y., Venkataraju, K.U., Pradhan, K., Mende, C., Taranda, J., Turaga, S.C., Arganda-Carreras, I., Ng, L., Hawrylycz, M.J., Rockland, K.S., et al. (2015). Mapping social behavior-induced brain activation at cellular

resolution in the mouse. Cell Rep. *10*, 292–305. https://doi.org/10.1016/j.celrep.2014.12.014.

59. Kim, Y., Yang, G.R., Pradhan, K., Venkataraju, K.U., Bota, M., García Del Molino, L.C., Fitzgerald, G., Ram, K., He, M., Levine, J.M., et al. (2017). Brain-wide Maps Reveal Stereotyped Cell-Type-Based Cortical Architecture and Subcortical Sexual Dimorphism. Cell *171*, 456–469.e22. https://doi.org/10.1016/j.cell.2017.09.020.
60. Renier, N., Adams, E.L., Kirst, C., Wu, Z., Azevedo, R., Kohl, J., Autry, A.E., Kadiri, L., Umadevi Venkataraju, K., Zhou, Y., et al. (2016). Mapping of Brain Activity by Automated Volume Analysis of Immediate Early Genes. Cell *165*, 1789–1802. https://doi.org/10.1016/j.cell.2016.05.007.
61. Behringer, R., Gertsenstein, M., Nagy, K.V., and Nagy, A. (2014). Manipulating the Mouse Embryo: a Laboratory Manual (Cold Spring Harbor Laboratory Press).
62. Sunkin, S.M., Ng, L., Lau, C., Dolbeare, T., Gilbert, T.L., Thompson, C.L., Hawrylycz, M., and Dang, C. (2013). Allen Brain Atlas: An integrated spatio-temporal portal for exploring the central nervous system. Nucleic Acids Res. *41*, D996–D1008. https://doi.org/10.1093/nar/gks1042.

STAR★METHODS

KEY RESOURCES TABLE

REAGENT or RESOURCE	SOURCE	IDENTIFIER
Antibodies		
Rabbit α-KsO	MBL	Cat#PM051M, RRID:AB_2876863
Mouse α-BrdU	BD Biosciences	Cat#555627, RRID:AB_395993
Mouse α-Oct3/4	Santa Cruz	Cat#sc-5279, RRID:AB_628051
Mouse α-Sox2	Santa Cruz	Cat#sc-365823, RRID:AB_10842165
Mouse α-SSEA-1	Santa Cruz	Cat#sc-21702, RRID:AB_626918
Goat α-Nanog	R&D Systems	Cat#AF2729, RRID:AB_2150103
Chicken α-GFP	Invitrogen	Cat#A10262, RRID:AB_2534023
Goat α-OMP	Wako	Cat#544-10001, RRID:AB_2315007
Rabbit α-TH	Pel-Freez	Cat#P40101-150, RRID:AB_2617184
Rabbit α-c-Fos	Cell Signaling	Cat#2250S, RRID:AB_2247211
Rabbit α-Egr	Santa Cruz	Cat#sc-189, RRID:AB_2231020
AF488 Goat α-Chicken	Abcam	Cat# ab150169, RRID:AB_2636803
AF488 Donkey α-Mouse	Molecular Probes	Cat# A-21202, RRID:AB_141607
BP-FITC α-Mouse IgGκ	Santa Cruz	Cat# sc-516140
AF488 Donkey α-Rabbit IgG	Molecular Probes	Cat# A-21206, RRID:AB_2535792
AF555 Donkey α-Mouse IgG	Thermo Fisher	Cat# A-31570, RRID:AB_2536180
AF555 Donkey α-Rabbit IgG	Molecular Probes	Cat# A-31572, RRID:AB_162543
AF647 Donkey α-Goat IgG	Abcam	Cat# ab150131, RRID:AB_2732857
Chemicals, Peptides and Recombinant Proteins		
DMEM	Gibco	Cat# 10566016
Fetal Bovine Serum	GeminiBio	Cat# 900-208-500
Penicillin-Streptomycin	Gibco	Cat# 15140122
Mitomycin C	Stemcell Tech.	Cat# 100-1048
DMEM/F-12	Gibco	Cat# 11320033
B-27 minus Vitamin A	Gibco	Cat# 12587010
N-2	Gibco	Cat# 17502048
Neurobasal-A	Gibco	Cat# 10888022
2-Mercaptoethanol	Gibco	Cat# 21985023
Mouse LIF	Stemcell Tech.	Cat# 78056
CHIR99021	Stemcell Tech.	Cat# 72054
PD0325901	Stemcell Tech.	Cat# 72184
TrypLE Express	Gibco	Cat# 124605010
Low Melt Agarose	Bio-Rad	Cat# 1613111
Sucrose	Acros Organics	Cat# EW-88356-95
0.5M EDTA	Invitrogen	Cat# 15575020
Tissue-TEK O.C.T Compound	Sakura	Cat# 4583
Triton X-100	Sigma-Aldrich	Cat# X100-100ML
BrdU	Invitrogen	Cat# B23151
EdU	Invitrogen	Cat# A10044
Sucrose	Millipore	Cat# S0389
Sodium Chloride	Millipore	Cat# S9888
Sodium bicarbonate	Millipore	Cat# S6014
D(+) Glucose	Millipore	Cat# G8270
Sodium dihydrogen phosphate monohydrate	Millipore	Cat# 1063460500

(*Continued on next page*)

Continued

REAGENT or RESOURCE	SOURCE	IDENTIFIER
Potassium chloride	Honeywell	Cat# 7447-40-7
Magnesium chloride hexahydrate	Honeywell	Cat# 7791-18-6
Calcium chloride hexahydrate	Honeywell	Cat# 7774-34-7
Potassium gluconate	Sigma-Aldrich	Cat# P1847
Phosphocreatine disodium salt hydrate	Sigma-Aldrich	Cat# P7936
HEPES	Sigma-Aldrich	Cat# H4034
Adenosine 5′-triphosphate disodium salt hydrate	Sigma-Aldrich	Cat# A26209
Guanosine 5′-triphosphate sodium salt hydrate	Sigma-Aldrich	Cat# 51120
EGTA/AM	Sigma-Aldrich	Cat# 324628
NBQX disodium salt	Biotechne Tocris	Cat# 479347-86-9
(R)-CPP	Biotechne Tocris	Cat# 02-471-0
Heparin	Sigma-Aldrich	Cat# H0200000
Glutaraldehyde	EMS	Cat# 16000
Glycine	Sigma-Aldrich	Cat# 50046
Ammonium chloride 20 mM	Sigma-Aldrich	Cat# 07781
Sodium cacodylate buffer	Sigma-Aldrich	Cat# 97068
Osmium teroxide	EMS	Cat# 19100
UranyLess EM Stain	EMS	Cat# 22409
Critical Commercial Assays		
Superscript IV Reverse Transcriptase	Invitrogen	Cat# 18090010
Zero Blunt TOPO PCR Cloning Kit for Sequencing	Invitrogen	Cat# 450159
Click-iT™ EdU Cell Proliferation Kit for Imaging, Alexa Fluor™ 488	Invitrogen	Cat# C10337
Experimental Models: Cell Lines		
Rat embryonic fibroblasts (REFs)	ATCC	Cat# CRL-1213
Experimental Models: Organisms/Strains		
OMP-IRES-Cre mice	Jackson Laboratory	RRID:IMSR_JAX:006668
TeNT-GFP mice	Provided by Martin Goulding	N/A
ROSA-DTA mice	Jackson Laboratory	Cat# 009669
C57BL/6J mice	Jackson Laboratory	Cat# 000664
Oligonucleotides		
Genotyping OMP mice WT Sense: 5'–TGTATTTCCTCATCACCTTTGGCG–3'	This study	N/A
Genotyping OMP mice WT Antisense: 5'–GGTCAGTCTCTTATCTCTCAGTCCCG–3'	This study	N/A
Genotyping OMP mice Cre Sense: 5'–CGATGCAACGAGTGATGAGGT–3'	This study	N/A
Genotyping OMP mice Cre Antisense: 5'–CGCATAACCAGTGAAACAGCA–3'	This study	N/A
Recombinant DNA		
Syn-hChR2(H134R)-eYFP	Zhang et al.[22]	Addgene Cat# 20945
pRRE	Dull et al.[46]	Addgene Cat# 12251
pRev	Dull et al.[46]	Addgene Cat# 12253
pMD2.G	Didier Trono	Addgene Cat# 12259
Software and Algorithms		
Elastix registration toolbox[47,48]	Klein et al.[47] Mattes et al.[48]	https://elastix.lumc.nl/
Prism 8	Graphpad	https://graphpad-prism.software.informer.com/8.0/
Custom Code	This study	https://doi.org/10.5281/zenodo.10880165

(*Continued on next page*)

Continued

REAGENT or RESOURCE	SOURCE	IDENTIFIER
Other		
Leica VT1000S	Leica	N/A
Leica CM3050 S	Leica	N/A

RESOURCE AVAILABILITY

Lead contact

Further information and requests for resources and reagents should be directed to and will be fulfilled by the lead contact, Kristin Baldwin (kb238@cumc.columbia.edu).

Materials availability

The materials used in this study, including the plasmids, mouse lines, cell lines and PSCs, are available upon request from the lead contact.

Data and code availability

- Microscopy and all other data reported in this paper will be shared by the lead contact upon request.
- The original code used to analyze the imaging data has been deposited on Github at: https://github.com/rmunozca/LSFM_ChimerasBrainRegistration https://doi.org/10.5281/zenodo.10880165
- Any additional information required to reanalyze the data reported in this paper is available from the lead contact upon request.

EXPERIMENTAL MODEL AND STUDY PARTICIPANT DETAILS

Mouse strains

CD-1 animals were used for surrogate mothers and to generate mouse embryonic fibroblast (MEF) feeder cells. Omp-IRES-Cre[29] mice were obtained from the Axel laboratory and crossed with C57BL/6J mice to generate heterozygotes. The TeNT-GFP mouse strain (TeNT) was previously provided by Martin Goulding[49] and ROSA-DTA (DTA) mice were ordered from The Jackson Laboratory (Stock # 009669).[50] Omp-IRES-Cre x C57BL/6J F_1 mice were bred with either TeNT or DTA mice to generate transgenic blastocysts and internal wild-type littermate controls. DBA/2J mice were crossed with C57BL/6J mice to generate C57BL/6J x DBA F_1 males for WT blastocyst generation and resulting chimeras were used for electrophysiology and birth dating experiments.[51] Both females and males were used for all experiments as noted, with only females used as hosts or donors for generation of chimeras, as is necessary. All animal experiments were conducted in accordance with the protocols approved by the IACUC of the host institutes in accordance with NIH guidelines for animal use. Animals were housed in the IACUC approved animal facilities of each Institute under the care and supervision of trained veterinary staff according to approved IACUC guidelines.

Cell culture conditions

HEK293T cells, MEFs, and rat embryonic fibroblasts (REFs) were cultured in standard media (DMEM with GlutaMAX, Gibco), 10% heat-inactivated fetal bovine serum (Gemini Bio), 1X penicillin-streptomycin, Gibco). MEF feeders were inactivated at passage 4 with chemical treatment of 1 μg/ml mitomycin-c (STEMCELL Technologies) overnight. MEFs and REFs were generated from litters containing both sexes and are therefore mixed. PSC cell lines used were all male due to improved stability of PSC lines. Rat PSCs were cultured on mitotically inactivated MEFs in serum-free 2i media (N2B27 basal medium 1:1 DMEM/F12, Gibco), N2 supplement (Gibco): Neurobasal A (Gibco), B27 supplement minus vitamin A (Gibco), 100 μM β-mercaptoethanol (Gibco)], supplemented with 10 ng/mL mouse LIF (STEMCELL Technologies), 3 μM CHIR99021 (STEMCELL Technologies), 1 μM PD0325901 (STEMCELL Technologies) and passaged as single cells onto fresh feeders using TrypLE Express (Gibco). All cells were kept at 37°C in a humidified environment at 5% CO_2. Non-commercial cell lines were authenticated by PCR and tested annually for mycoplasma.

METHOD DETAILS

Generation of chimeras

DAC2 and DAC8 cells lines were provided by the Ying laboratory.[3,12] SDFE and SDFF rat iPSC lines were previously reported.[3] SDMJ rat iPSC lines were generated by the Belmonte lab and SD riPSC 9.3 by the Baldwin lab. The mouse PSC line (31-2/B2) was previously generated by the Baldwin lab.[52] Chimeras were produced by injection of PSC cells into E3.5 blastocysts, collected from superovulated C57BL/6J females mated to C57BL/6J x DBA2 F_1 stud males, as previously reported,[3,44,53] or into E3.5 transgenic and WT (control) blastocysts, generated by transgenic mouse crossings, described above in "mouse strains" section.

Tissue preparation and immunostaining

Mice at P21 were euthanized with isoflurane and transcardially perfused with 4% PFA (EMS). Brains with OBs attached, and the OE were dissected from the skull and placed in 4% PFA solution overnight at 4°C. For mice at P10 and younger, animals were briefly anesthetized, decapitated, and the entire head fixed in 4% PFA solution overnight at 4°C. After post-fixation, brains were washed in PBS. Cells in culture were washed and then fixed in 4% PFA for 10 min at room temperature.

For vibratome sections, brains were embedded in 4% low-melt agarose (Bio-Rad) and sectioned in the coronal plane at 80 μm using a Leica VT1000S. For cryostat sections, samples were submerged in 30% sucrose (Acros Organics) at 4°C and left overnight or until the tissue sank to the bottom of the tube. OE samples from mice P21 and older were incubated in 0.5 M EDTA solution, pH 8.0 (Invitrogen) for 1 hr. at room temperature to decalcify before dehydrating in 30% sucrose. Dehydrated samples were embedded in Tissue-Tek O.C.T. (Sakura), rapidly frozen in a bath of 70% ethanol and dry ice, and stored at -80°C. Before sectioning, samples were moved to -20°C for 1 hr. Using a Leica CM3050 S, 30 μm cryosections were collected and allowed to air dry for 1 hr. before staining or storage at -80°C.

For IHC and ICC, vibratome or cell culture samples were blocked in 10% heat-inactivated horse serum (Lonza BioWhittaker) and 0.1% Triton X-100 (Sigma-Aldrich) for 1 hr. at room temperature. Primary antibodies were diluted 1:500 (IHC) or 1:250 (ICC) in blocking buffer and added overnight at 4°C. Sections were washed three times and then stained with secondary antibodies and DAPI (5 mg/ml), both diluted 1:1,000 in 0.1% Triton X-100, for 1 hr. at room temperature. Cryosections followed the same protocol with a few additions. Slices were removed from -80°C and brought to room temperature for ∼30 min. In cases of antigen retrieval (AR), slides were submerged in sodium citrate buffer (Sigma Aldrich) warmed to ∼85-90°C on a hot plate for 20 min. All sections were washed twice to rehydrate samples and remove residual O.C.T. before blocking.

The following primary antibodies were used: KsO (MBL PM051M, Rabbit, Polyclonal, IHC), BrdU (BD Pharmingen 555627, Mouse, Monoclonal, IHC – HCl treatment), Oct4 (SCBT sc-5279, Mouse, Monoclonal, ICC), Sox2 (SCBT sc-365823, Mouse, Monoclonal, ICC), SSEA1 (SCBT sc-21702, Mouse, Monoclonal, ICC), Nanog (R&D Systems AF2729, Goat, Polyclonal, ICC), GFP (Invitrogen A10262, Chicken, Polyclonal, ICC – 1:500), OMP (Wako 544-10001, Goat, Polyclonal, IHC – AR), TH (Pel-Freez P40101-150, Rabbit, Polyclonal, IHC), cFos (CST 2250S, Rabbit, Monoclonal, IHC), and Egr1 (SCBT sc-189, Rabbit, Polyclonal, IHC). The following secondary antibodies were used: Alexa Fluor 488 (Abcam ab150169, Goat anti-Chicken IgY H&L), Alexa Fluor 488 (Invitrogen A-21202, Donkey anti-Mouse IgG H&L), BP-FITC (SCBT sc-516140, anti-Mouse IgGκ), Alexa Fluor 488 (Invitrogen A-21206, Donkey anti-Rabbit IgG H&L), Alexa Fluor 555 (Invitrogen A-31570, Donkey anti-Mouse IgG H&L), Alexa Fluor 555 (Invitrogen A-31570, Donkey anti-Mouse IgG H&L), Alexa Fluor 555 (Invitrogen A-31572, Donkey anti-Rabbit IgG H&L), and Alexa Fluor 647 (Abcam ab150131, Donkey anti-Goat IgG H&L).

Nucleic acid extraction and PCR

Genomic DNA was extracted from mouse tail tip samples using the REDExtract-N-Amp Tissue PCR kit (Sigma-Aldrich). PCR was performed using the REDExtract-N-Amp PCR Readymix (Sigma-Aldrich). The following primers were used for genotyping: *Omp* WT Sense: 5'–TGTATTTCCTCATCACCTTTGGCG–3'; *Omp* WT Antisense: 5'–GGTCAGTCTCTTATCTCTCAGTCCCG–3'; Cre Sense: 5'–CGATGCAACGAGTGATGAGGT–3'; Cre Antisense: 5'–CGCATAACCAGTGAAACAGCA–3'.

For species genotyping and validating hSyn-ChR2-eYFP subclones, genomic DNA was extracted from rat PSC cell pellets using the DNeasy Blood and Tissue kit (Qiagen) and PCR was performed using the Platinum PCR SuperMix High-Fidelity kit (Invitrogen). Rat PSC lines were validated by genotyping for the rat specific *Omp* allele using the following primers: *Omp* Mouse Sense: 5'–CCTGACAGGGGCTATGACAGAGTG–3'; *Omp* Rat Sense: 5'–GGCAGTATGCGGTTGGATCAATCAG–3'; *Omp* Common Antisense: 5'–CCTGGTCCAGAACCAGCGGC–3'. To validate hSyn-ChR2-eYFP insertion within subclones, the following primer sets were used for ChR2: ChR2 Sense 1: 5'–GGATTGAATCTCGCGGCACG–3'; ChR2 Antisense 1: 5'–GTTGCCATGGCGCTGGTAGC–3'; ChR2 Sense 2: 5'–GCGTCCTGAGCGTCTATGGC–3'; ChR2 Antisense 2: 5'–GCTTGCCGGTGGTGCAGATG–3'; ChR2 Sense 3: 5'–GTTCA TCTGCACCACCGGCA–3'; ChR2 Antisense 3: 5'–GCACGCTGCCGTCCTCGATG–3'.

For RT-PCR, the following intron spanning primers were used to amplify a fragment of Syn1; Forward: 5'- AAG ACAAGC AGCTCATCGT – 3', Reverse: 5'- TGCTGGGAGGTCTGG – 3'. Superscript IV Reverse Transcriptase (Invitrogen) was used for the RT-PCR. Zero Blunt TOPO PCR Cloning Kit (Invitrogen) was used to clone and sequence the resulting PCR bands.

Lentiviral constructs and production

The Syn-hChR2(H134R)-eYFP lentiviral plasmid was ordered through Addgene (#20945).[22] The rtTAM2.2 cassette (rtTA) was generated previously[53] and cloned into a lentiviral transfer plasmid by the K. Baldwin laboratory.[51] Doxycycline (dox)-inducible lentiviral reprogramming factors encoding mouse cDNAs for Oct4, Sox2, c-Myc, and Klf4 were generated previously.[51] Virus was produced in HEK293T cells (ATCC CRL-3216) by calcium phosphate co-transfection of lentiviral shuttle and packaging vectors: pRRE (Addgene #12251), pRev (Addgene #12253), pMD2.G (Addgene #12259).[54,55] Live lentivirus was harvested 48 hr. post-transfection for transduction.

Rat iPSC reprogramming

Rat embryonic fibroblasts (REFs) from WT Sprague-Dawley rats were obtained from ATCC (CRL-1213) and reprogrammed into iPSCs using dox-inducible lentiviral vectors according to previously established protocols.[3,51] New rat iPSC lines were validated

by immunocytochemistry for pluripotency markers (Sox2, Oct4, SSEA1, Nanog) and their subsequent contribution to multiple mouse tissues in interspecies chimeras.

Lentiviral-integrated iPSC subclones

To generate riPSC::hSyn-ChR2-eYFP lines, iPSCs were separated from mitotically inactive MEF feeders by culturing on Matrigel-coated (Corning) tissue culture flasks for 3 passages. hSyn-hChR2(H134R)-eYFP lentivirus was added to single cells after the third passage and left overnight. The following day, lentivirus was removed, iPSCs were washed twice with phosphate-buffered saline (PBS), passaged, and then seeded at $5x10^5$ cells on fresh feeders in 10-cm^2 tissue culture dishes. Three days after seeding, subclones were manually picked using fluorescence as a guide, expanded, and validated for successful ChR2 integration by PCR.

Animal behavior assay

Animals P35 and older were used for the buried cookie assay. Animals were pre-exposed to a reward, specifically an Oreo Mini (Nabisco) chocolate cookie wafer without the icing, 4-5 days before the test was performed. Only animals that ate the cookie within 24 hours during the pre-exposure were used for further testing. Animals were moved to a clean cage and deprived of food overnight to increase motivation. For testing, clean static cages without a water port were filled with approximately 4 cm of fresh bedding and fitted with a clean filter top. During the test, the animals were placed in the clean cage for 10 min to allow them to habituate before returning them to their home cage. Meanwhile, half an Oreo Mini cookie without the filling was buried approximately 2 cm deep in the bedding in a random corner of the test cage. The animal was then placed in the test cage and the timer was started. Up to a maximum of three animals were tested at the same time in separate cages. A single trial ran for 15 min, or when the animal found the cookie and actively interacted with it by eating it or carrying it away. Animals that failed to locate the reward were shown the cookie and assessed for motivation. They were excluded from the final analysis if they did not interact with the reward. On the conclusion of the trial, the animal was returned to their home cage and provided with food.

Acute slice electrophysiology, recording, and analysis

WT chimeras were generated using riPSC::hSyn-ChR2-eYFP subclone #9.3 and used from 2-6 wks. of age for experiments. To isolate slices containing the hippocampus and cortex, animals were anesthetized briefly with isoflurane then decapitated. The skin and skull were removed to expose the brain, which was rapidly dissected out and placed in ice-cold sucrose cutting solution (100 mM Sucrose (Sigma-Aldrich), 60 mM NaCl (Sigma-Aldrich), 26 mM $NaHCO_3$ (Sigma-Aldrich), 20 mM D-Glucose (Sigma-Aldrich), 1.25 mM NaH_2PO_4-H_2O (Sigma-Aldrich), 2.5 mM KCl (Honeywell Research Chemicals), 5 mM $MgCl_2$-$6H_2O$ (Honeywell Research Chemicals), 1 mM $CaCl_2$ (Honeywell Research Chemicals)) bubbled with 95% O_2/5% CO_2. Blocking cuts were made to remove the CB and OBs, bisect the hemispheres, and orient Hipp in the transverse plane. The blocked tissue was transferred to the slicing chamber of a Leica VT1200S vibratome containing cold, oxygenated sucrose cutting solution. Isolated 300 μm thick slices were transferred to a recovery chamber containing ACSF (127 mM NaCl, 25 mM $NaHCO_3$, 25 mM D-Glucose, 1.25 mM NaH_2PO_4-H_2O, 2.5 mM KCl, 2 mM $CaCl_2$, 1 mM $MgCl_2$-$6H_2O$) bubbled with 95% O_2/5% CO_2 to recover for 30 min at 32°C and were then maintained at room temperature.

Slices were transferred to a recording chamber and perfused with oxygenated ACSF warmed to 31°C. Whole-cell current clamp recordings were obtained from eYFP-positive rat and eYFP-negative mouse neurons visualized using a Scientifica SliceScope fitted with a SciCamPro for infrared differential interference contrast (IR-DIC) and fluorescence optics. Patch pipettes (3-5 mΩ) were filled with potassium gluconate internal solution (130 mM K-gluconate (Sigma-Aldrich), 11.5 mM Na_2-phosphocreatine (Sigma-Aldrich), 10 mM HEPES (Sigma-Aldrich), 3 mM $MgCl_2$, 3 mM Na_2-ATP (Sigma-Aldrich), 0.2 mM Na-GTP (Sigma-Aldrich), 0.2 mM EGTA (Sigma-Aldrich), pH = 7.2, osmolarity = 307 mOsm). Current was applied to maintain cells at -70 mV and series resistance was monitored throughout recordings. Experiments were discarded if the holding current was greater than -300 pA, if the series resistance was greater than 25 MΩ, or if the series resistance changed by more than 20%. All recordings were acquired using a Multiclamp 700B amplifier and ScanImage software.[56] Signals were sampled at 10 kHz and filtered at 6 kHz. Analysis was performed using IGOR Pro (WaveMetrics).

Light-evoked EPSPs were triggered by illumination with a blue LED in 2 ms epochs every 3 sec. LED intensity was set to the minimum necessary to evoke the maximum amplitude EPSP. The average baseline EPSP was established with a minimum of 20 sweeps before adding glutamate receptor antagonists (10 μM NBQX (Tocris) and 10 μM CPP (Tocris)) to the bath to block synaptic currents. Responses were monitored as antagonists washed in, and once the EPSP was blocked (~3 min), a minimum of 20 sweeps were recorded. EPSP amplitudes were calculated by averaging the amplitude 0.5 ms before to 2 ms after the peak of the current.

Dual-pulse birth dating, staining, and analysis

Pregnant surrogates were given intraperitoneal injections delivering 50 mg/kg of BrdU (Life Technologies) at E12.5 and 50 mg/kg of EdU (Life Technologies) at either E13.5, E14.5, or E17.5 to label neurons in developing WT chimera embryos. Reconstituted as 10 mg/ml (BrdU) and 5 mg/ml (EdU) in dPBS, this equated to 200 μl and 400 μl injections, respectively, for a 40 g mouse. Chimeric brains were harvested at 4 wks. for IHC as described above.

For BrdU-EdU double staining, the following modifications were made to the IHC protocol. Slices were pre-stained with the KsO antibody in blocking buffer overnight at 4°C. Slices were washed three times, fixed again with 4% PFA for 15 min at room

temperature, washed, and incubated in preheated 1N HCl solution for 30 min at 37°C. To neutralize, 0.1 M sodium borate buffer pH 8.5 was added at room temperature for 10 min. Slices were washed twice, blocked for 1 hr., and stained overnight at 4°C with BrdU and KsO primary antibodies. The subsequent day, slices were washed, stained with secondary antibodies, and then mounted onto slides to dry for 15 min at room temperature. The Click-iT EdU Cell Proliferation Kit for Imaging (Invitrogen) was used to identify EdU-positive cells following the manufacturer's instructions starting with step 4.1 except 0.1% Triton X-100 was substituted for 3% BSA, slides were incubated with the reaction cocktail for 1 hr., and were stained for DAPI in 0.1% Triton X-100 for 1 hr.

To calculate the location of EdU-positive cortical cells, an arc was drawn to mark the border between cortex and corpus callosum (CC). Neurons were manually identified, sorted by KsO double staining, and their shortest distance to the marked border measured. For BrdU-EdU double staining, EdU-positive and BrdU-positive/EdU-negative labelled cells were manually identified and sorted by KsO expression. Cell densities were normalized to an average density of DAPI-stained nuclei (mouse) or the density of KsO-positive (rat) cells present in corresponding regions. Average DAPI densities were generated by counting the area ~250 DAPI-stained nuclei occupy across 8 samples. Analysis was performed using R (3.5.1) and Prism 8 (GraphPad).

Transmission Electron Microscopy

Mice were anesthetized with isoflurane and prepared for transcardial perfusion. First, Ringer's solution (125 mM NaCl, 1.5 mM $CaCl_2$, 5 mM KCl, 0.8 mM Na_2HPO_4, 20,000 units of heparin (Sigma-Aldrich), pH 7.4) bubbled with 95% O_2/5% CO_2 and warmed to 40°C was perfused using a peristaltic pump through the heart, followed by fixative solution containing 4% PFA and 0.25% glutaraldehyde (EMS) in warm PBS. Brains with OBs attached were dissected from the skull and placed in fixative solution at room temperature for 2 hours, then 4°C overnight. The following day, samples were washed three times in fresh PBS, once in PBS with glycine (50 mM) for 10 min, and then returned to PBS. After washing, intact brains were embedded in 4% low-melt agarose and sectioned in the coronal plane at 50 μm. Free-floating olfactory bulb sections were visually screened with fluorescence to identify those containing rat glomeruli.

Olfactory bulb sections containing rat glomeruli were treated with glycine (50 mM, Sigma-Aldrich) and ammonium chloride (50 mM, Sigma-Aldrich) in PBS for 5 min, blocked with 10% albumin for 1 hour, and incubated with primary KsO antibody overnight at 4°C. The following day, sections were washed three times for 20 minutes each in 1% albumin-PBS, incubated with secondary antibody coupled with 1 nm gold particles (Nanoprobe) for 40 min, washed an additional three times in albumin-PBS, and post-fixed with 4% PFA, 2.5% glutaraldehyde, 100 mM cacocylate buffer (Sigma-Aldrich) for 20 min at 4°C. Then samples were washed in the same buffer three times, post-fixed with 1% osmium tetroxide (EMS) and 1.2% potassium ferrocyanide in 100 mM cacodylate buffer for 40 min and washed an additional three times. Sections were dehydrated in an acetone series until 100% (3x) and embedded in Epon resin. Ultrathin sections of 50 nm were obtained with a diamond knife (Diatome) and collected on 300 mesh nickel grids. A silver-enhancement step using Aurion SE-EM kit was performed for 30 min to enlarge the nanogold particles to 8-10 nm size and enhance visualization on the TEM. Finally, sections were post-stained with UranyLess (EMS) for 5 min to improve contrast and observed in a Zeiss Libra 120 operated at 80 kV. High-resolution images (4K x 4K) were obtained with a CCD camera Gatan US4000.

Whole-brain image acquisition

Animals were perfused, brains post-fixed overnight with 4% PFA, and samples cleared using a water-based high-refractive index clearing solution (Z.W., unpublished data). The cleared brains were imaged on a commercial light-sheet microscope (Zeiss Z.1 Light-sheet), equipped with two 10× illumination objectives (0.2 NA) and a 5× detection objective (0.16 NA), at a pixel x-y-z resolution 1.26 × 1.26 × 8.04 mm. Every optical section was acquired as a tiled mosaic, with 488 nm and 561 nm channels scanned sequentially.

QUANTIFICATION AND STATISTICAL ANALYSIS

Confocal imaging, image processing, and analysis

All images were acquired on a Nikon A1 confocal microscope as large-image z-stacks. Analysis was performed using Nikon NIS-Elements. To count glomeruli, circular spaces were identified in the glomerular layer (GL) devoid of DAPI staining. For glomerular counts in P10 chimeras, glomeruli were manually counted across 32 serial sections and the total normalized to the hemisphere with no rat OSNs for each animal. To calculate the area of the GL, maximal coronal sections just anterior to the accessory olfactory bulb were used. Using DAPI counterstaining as a guide, the interior and outer edges of the GL (omitting the olfactory nerve layer) were traced, and the difference between these areas was calculated. For glomerular area in 7-14 wk. adult mice, borders were drawn for each glomerulus following DAPI and sorted by KsO expression. For TH intensity, glomeruli were outlined and the integrated density calculated using Fiji.[57] Cell counts (OMP, Egr1, cFos) were done manually in respective neuronal layers. The OE was defined using DAPI as the region between the lumen and lamina propria, and layer 2 of PCx as the dense band of nuclei. For IEG staining in PCx, serial sections were collected from the OB through PCx on the cryostat in order to maintain brain orientation. OB sections were visualized to identify animals with unilateral rat OSN contribution and to which hemisphere. Cortical sections were subsequently stained for cFos and Egr1, imaged, and cells manually counted within layer 2 of PCx. Cell densities were normalized within each slice to the hemisphere without rat OSN contribution. Statistical analyses were run using Prism 8 (GraphPad).

ROI Brain Area Analysis

Anatomical-based segmentation of the 3D registered brains was done using the 2011 Allen Reference Brain Atlas (ARA) labels with modifications as previously described . The developmental origin based segmentation was achieved using the Allen Developing Mouse Brain Atlas labels[54] registered to the RSTP brain as described above for whole-brain registration, with the transformation parameters obtained from the standardized RSTP brain applied to warp and align the atlas onto the chimera brains.

Whole-brain registration

Imaged brains from 6-8 wk., mixed sex chimeras were registered to a standardized mouse reference STP (RSTP) brain as previously described.[58–60] Initial 3D affine transformation was calculated using 6 resolution levels, followed by a 3D B-spline transformation with 3 resolution levels. Similarity was computed using Advanced Mattes mutual Information metric by *Elastix* registration toolbox.[61,62] In order to enhance the precision of the image registration, both the acquired brain images and the reference brain were pre-processed used custom scripts to enhance anatomical landmark features used in the computation of mutual information, available at https://github.com/rmunozca/LSFM_ChimerasBrainRegistration.

Brain Signal Segmentation

Whole brain signal distribution of the KsO-labeled rat cells was automatically detected using custom scripts. First, the signal background was reduced using a gamma correction filter and the signal threshold was set using Otsu's algorithm; second, pixels detected were located in the 3D brain coordinates and mapped onto the anatomical brain areas of the reference atlases; third, the signal was quantified as the number of pixels per anatomical regions either in the standard ARA atlas or in the Allen Developing Mouse Brain Atlas; finally, the density analysis was expressed as the pixel volume per brain area volume for all anatomical regions as described previously.[40,41] All quantifications were done separately for each hemisphere.

Statistical Analyses

Details of each statistical analyses are provided in the main text and in the figure legends. All analyses were performed after determining whether the distribution of the data met the assumptions of the test. Determination of the rat vs. mouse identity for the electron microscopy was performed blinded by the core director. Behavioral experiments were scored blind to the genotype or chimeric status. Quantification of labelled co-labeled cells in brain slices were performed with coded slides such that the genotypes were not known until counts were complete.

CellPress

Supplemental figures

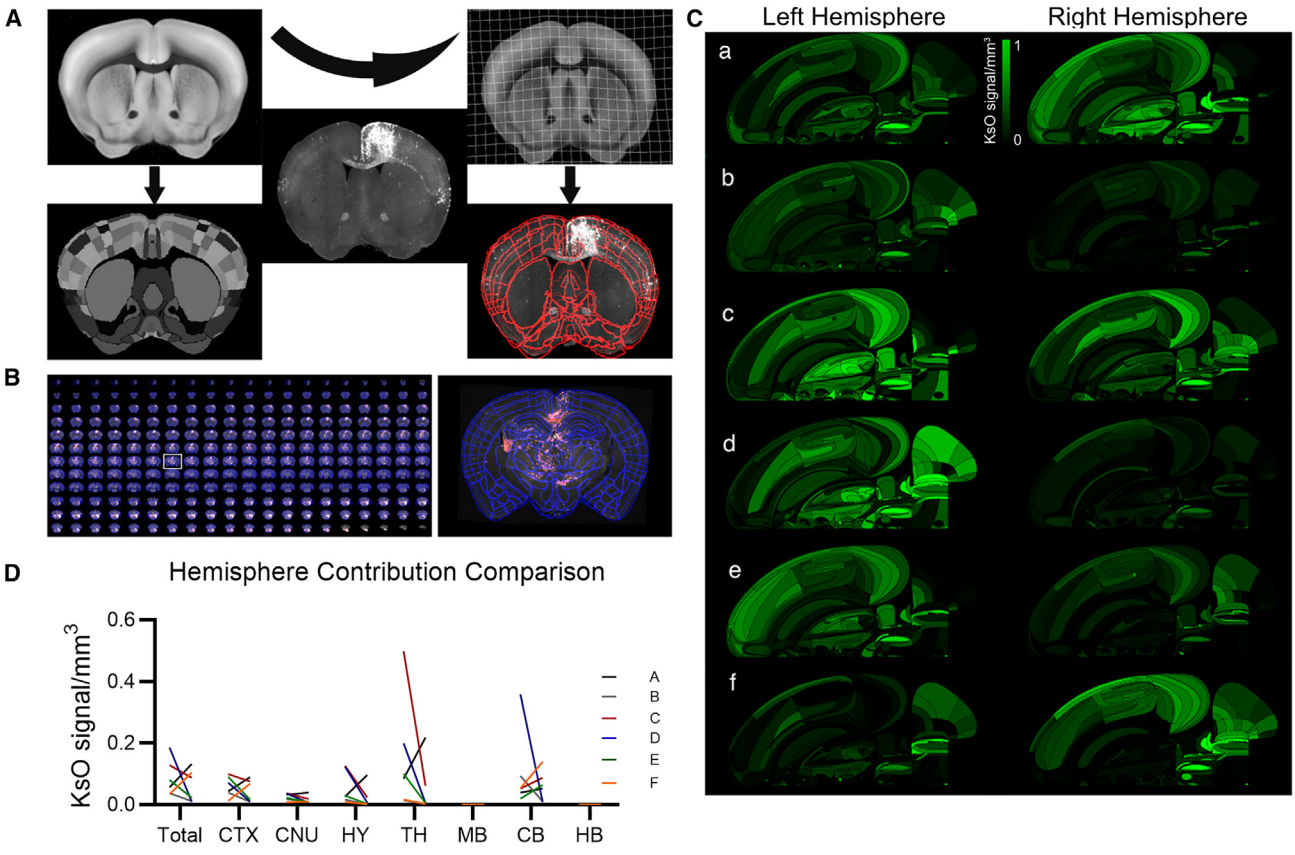

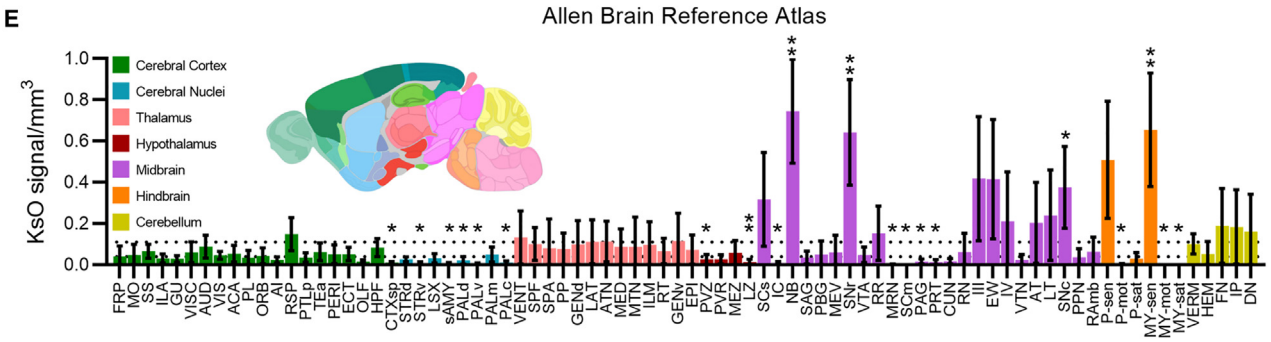

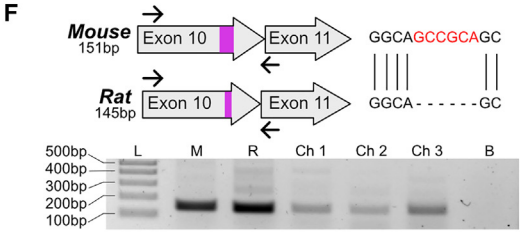

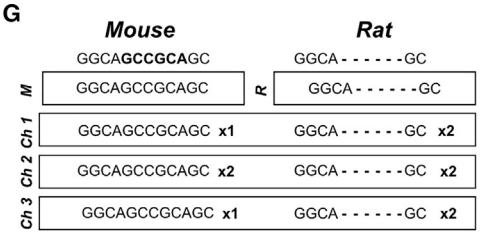

(legend on next page)

Figure S1. Whole-brain volumetric analysis, related to Figure 1

(A) Schematic of whole-brain imaging and registration workflow. After imaging, brains were aligned to a reference atlas, and KsO signal was detected and registered within each region.

(B) Serial coronal images depict KsO signal within registered regions. White outline indicates inset.

(C) Flat map projections of KsO signal for both hemispheres of each brain sample, $n = 6$ animals.

(D) Volumetric analysis between hemisphere comparison reveals bilateral KsO density asymmetry within the animal. Samples registered to the Allen Mouse Brain Reference Atlas. Sample ID (A)–(F) indicates that each chimera is matched to its own hemisphere and representative slices of these are shown in (C), where (a)–(f) are related to (A)–(F).

(E) Volumetric analysis of KsO expression in brain regions defined by the Allen Mouse Brain Reference Atlas.

(F) RT-PCR strategy to distinguish between rat and mouse Syn1 gene. Common primers targeted to mouse and rat Syn1 gene where the rat gene has a deletion (shown in red; top). RT-PCR was performed on RNA isolated from mouse (M), rat (R), rat-mouse chimera 1 (Ch1), rat-mouse chimera 2 (Ch2), rat-mouse chimera 3 (Ch3), and blank (B). Bands were observed at the expected size (approximately 150 bp).

(G) Bands from RT-PCR were then cloned and sequenced. Mouse and rat controls aligned with their respective sequences. From chimera 1, 3 colonies were successfully sequenced and then aligned (1 to mouse and 2 to rat sequence). From chimera 2, 4 colonies were successfully sequenced and then aligned (2 to mouse and 2 to rat). From chimera 3, 3 colonies were successfully sequenced and then aligned (1 to mouse and 2 to rat).

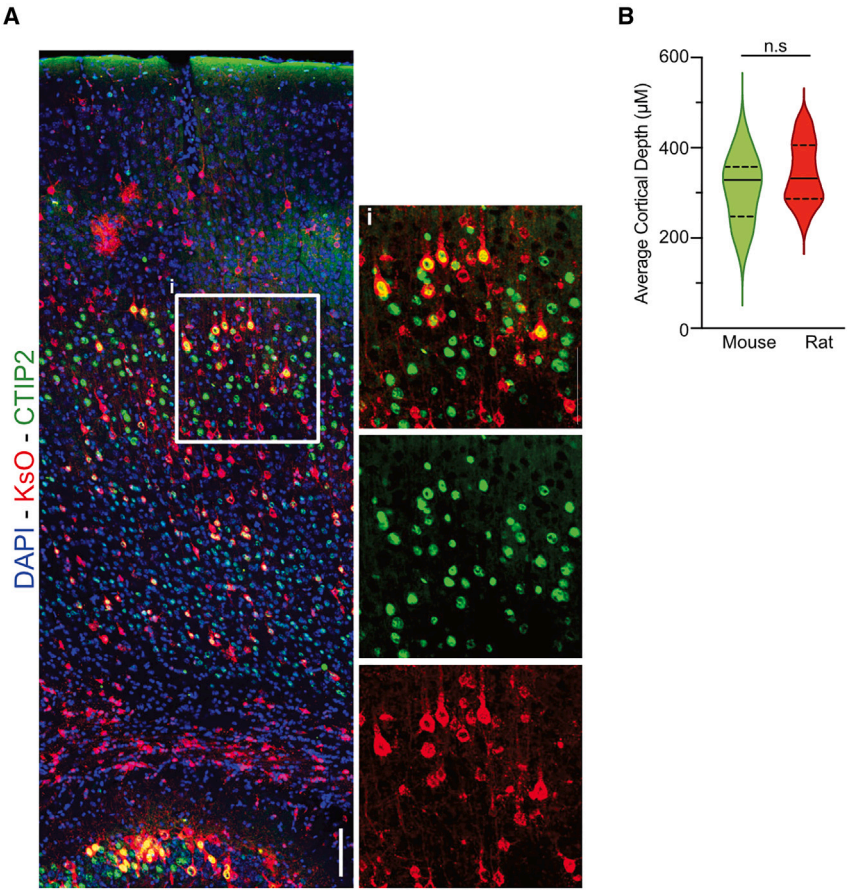

Figure S2. Development of rat cells in mouse brains, related to Figure 2

(A) Representative images of cortical CTIP2 staining in rat-mouse chimeras. Insets shown (right) represent the white box (left). Shown are nuclei (DAPI, blue), rat KsO cells (red), and CTIP2 (green). Scale bars, 100 μm.

(B) The distance to corpus callosum from the nucleus of each CTIP2-positive cell was measured, and CTIP2-positive rat cells (red, KsO) were compared with non-red CTIP2-positive mouse cells. The measured distances for mouse and rat cells were averaged per slice. *n* = 18 slices, 5 animals, and were not significantly different (two tailed, paired t test).

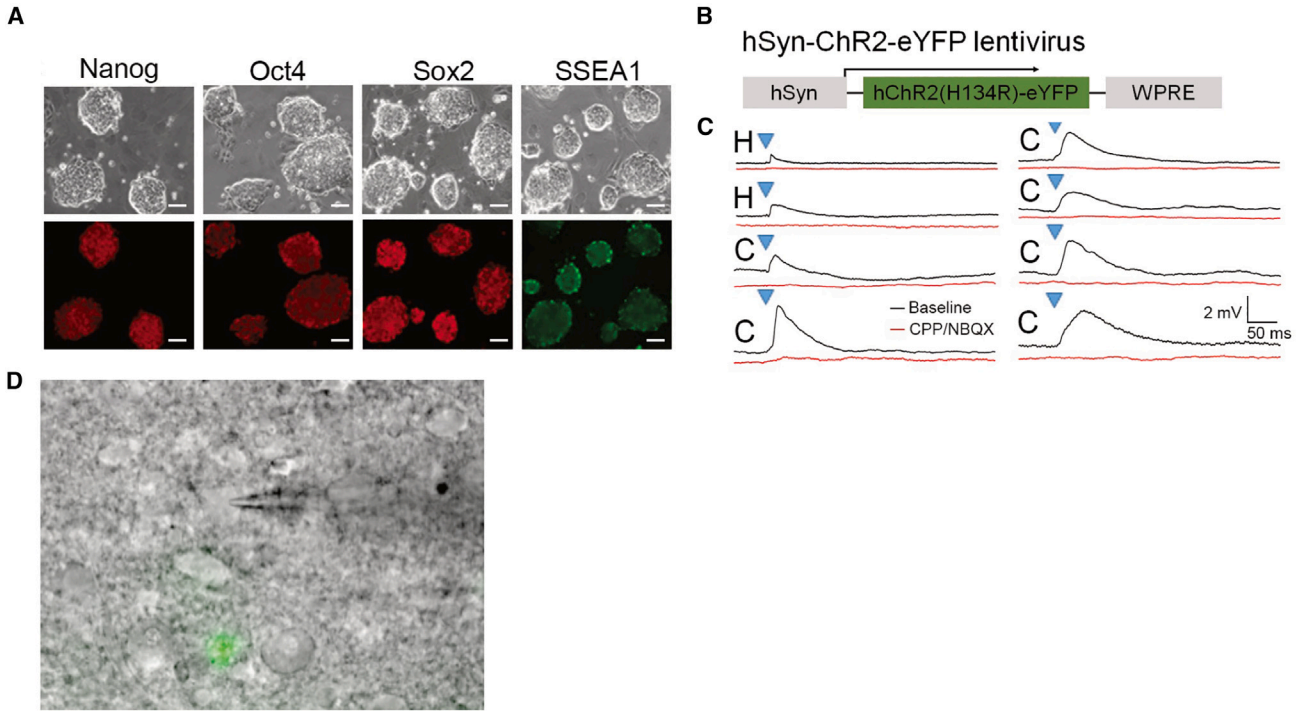

Figure S3. Rat-mouse synapses, related to Figure 3

(A) Expression of pluripotency marker genes Nanog, Oct4, Sox2, and SSEA1 in rat iPSCs carrying channelrhodopsin2 fused to the eYFP protein (hChR2H134R0-eYFP). Nanog, Oct4, and Sox2 are shown in red, and SSEA is shown in green. Scale bars, 50 μm.

(B) Schematic of lentiviral construct inserted in rat iPSCs. Expression of channelrhodopsin2 fused to the eYFP protein is driven by the human Synapsin promoter (hSyn) to enable high expression in neurons.

(C) Traces of light-evoked EPSPs in recorded mouse neurons. Blue triangles mark blue light stimulation. Traces are an average of 20 trials and shown are traces from cortex (C) and hippocampus (H). Scale bar is 2 mV, 50 ms. *n* = 10 YFP− mouse cells, 7 animals.

(D) Example of a recording from a mouse neuron (pipette) separated from the rat neuron by several cell bodies (green).

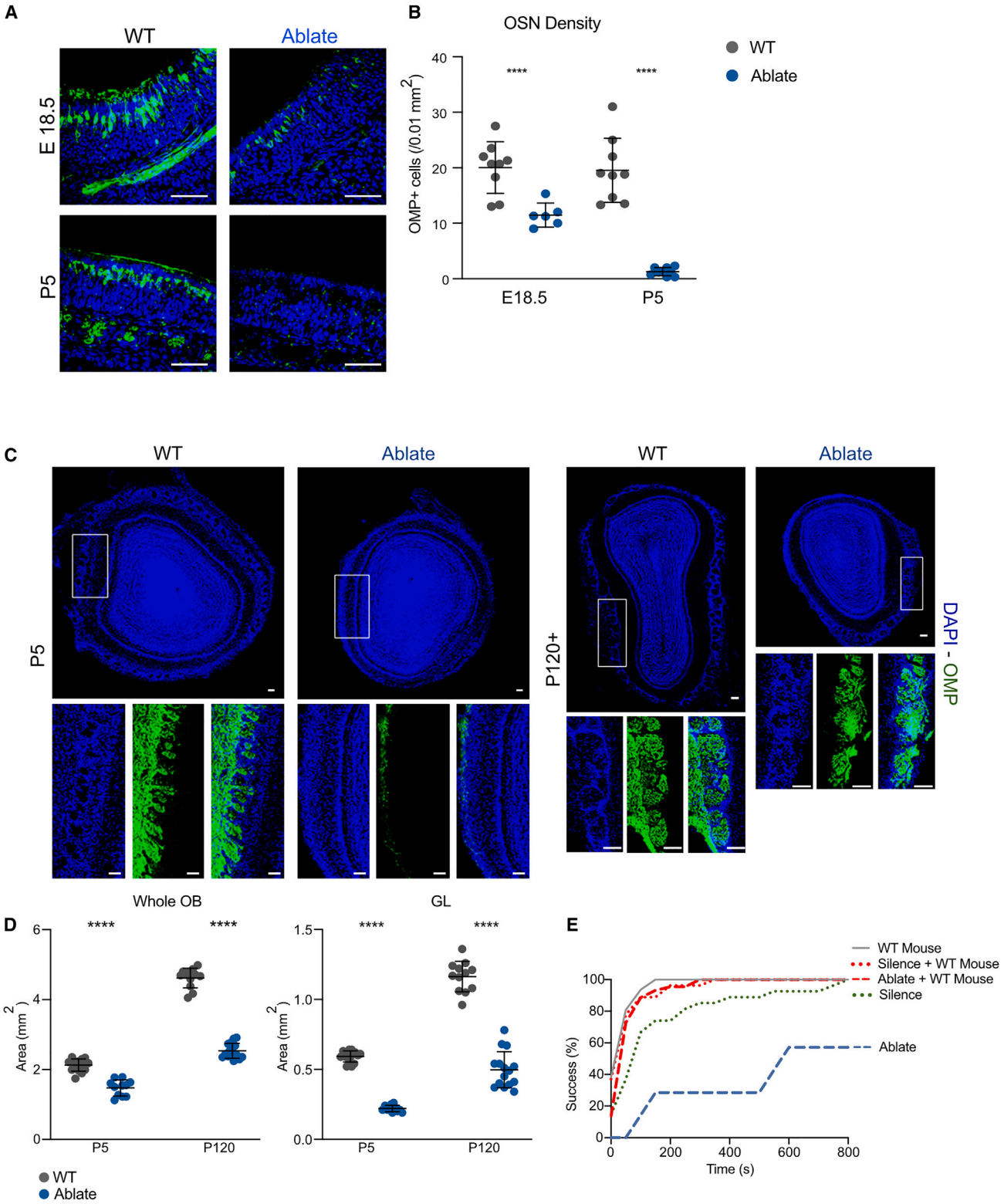

Figure S4. Genetic models of olfactory system disability for complementation studies, related to Figure 4

(A) Representative images of antibody staining for OMP (green) with nuclei (DAPI, blue) in the OE of E18.5 and P5 WT and Ablate mice. Scale bars, 100 μm.

(B) OMP+ OSNs are depleted in both E18.5 and P5 Ablate OEs. Data are mean ± 95% CI, $n = 2–3$ animals/genotype, 3 slices/animal. Significance was determined by two-way ANOVA and Sídák's multiple comparisons test, $^{***}p < 0.001$, $^{****}p < 0.0001$.

(legend continued on next page)

(C) Representative images showing OMP (green) density in P5 and P120+ mice for both WT and Ablate mice (DAPI, blue). Number of glomeruli are decreased in P5 Ablate mice but not completely absent in adult animals (P120+). Scale bars, 50 μm.

(D) The olfactory bulb (whole OB) and glomerular layer (GL) areas are smaller in Ablate mice at both P5 and P120+. Data are mean ± 95% CI, n = 4–5 animals/genotype, 3 slices/animal. Significance was determined by two-way ANOVA and Sídák's multiple comparisons test, ****$p < 0.0001$.

(E) WT mouse PSCs rescue behavior in both models. Shown are the percentage of the mice that found the cookie, plotted as cumulative success per second (s).

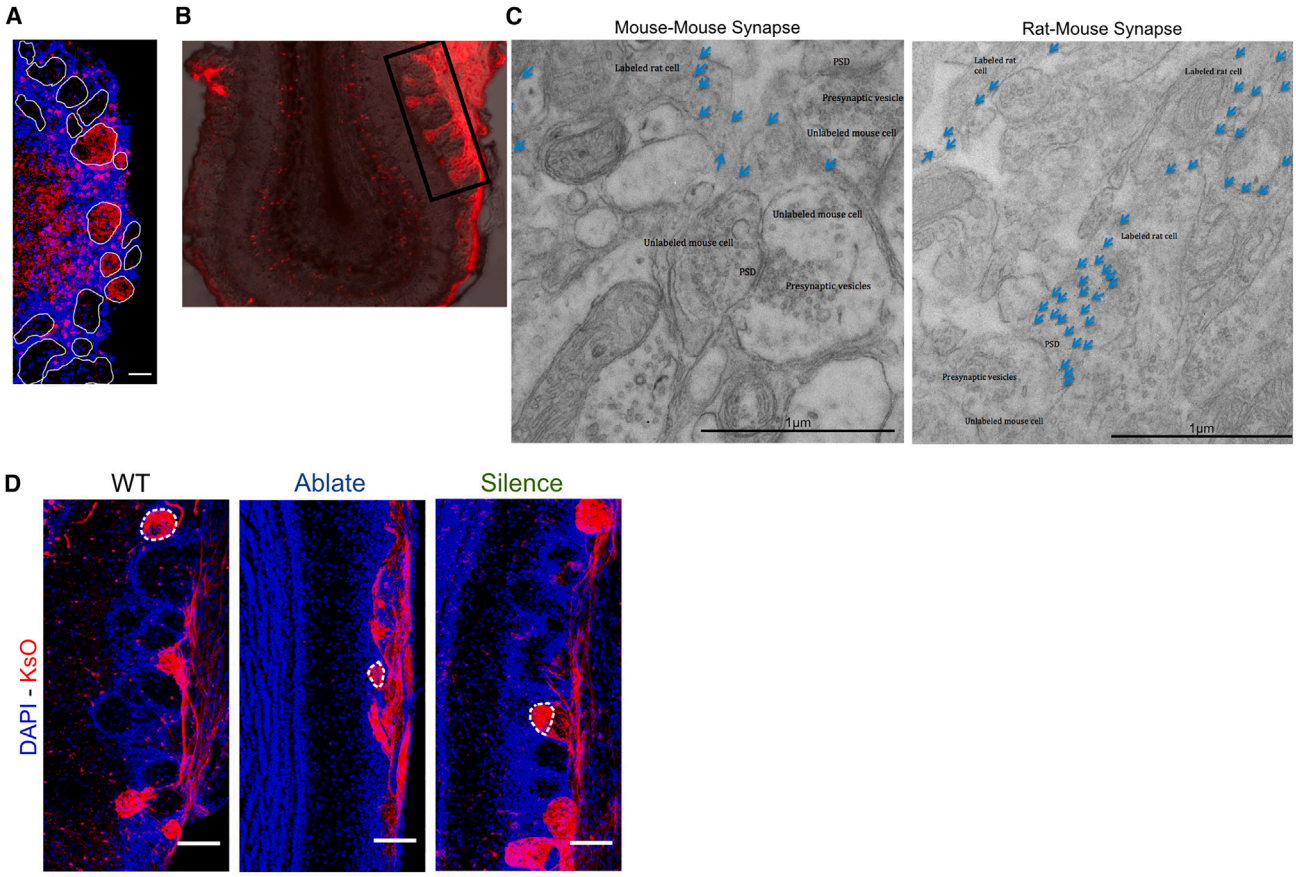

Figure S5. Rat OSN contribution to olfactory circuits, related to Figure 5

(A) Rat glomeruli are maintained in the olfactory bulb (OB) in aged mice. Shown are rat KsO (red) and nuclei (DAPI, blue) from an approximately 2-year-old mouse-rat chimera.

(B) Section of the OB used for transmission electron microscopy (TEM).

(C) Representative images of TEM of synapses in the OB. Scale bars, 50 μm. The electron microscopy images were examined from the area outline in the overview image of the OB (left, red is KsO expression from rat cells in a mouse OB). Examples of a mouse-mouse synapse (left) and a rat-mouse synapse (right) are shown.

(D) Rat glomeruli (red) in chimeras generated from each transgenic cross; nuclei in blue (DAPI) outline structures. Dotted lines outline glomeruli. Scale bars, 100 μm.

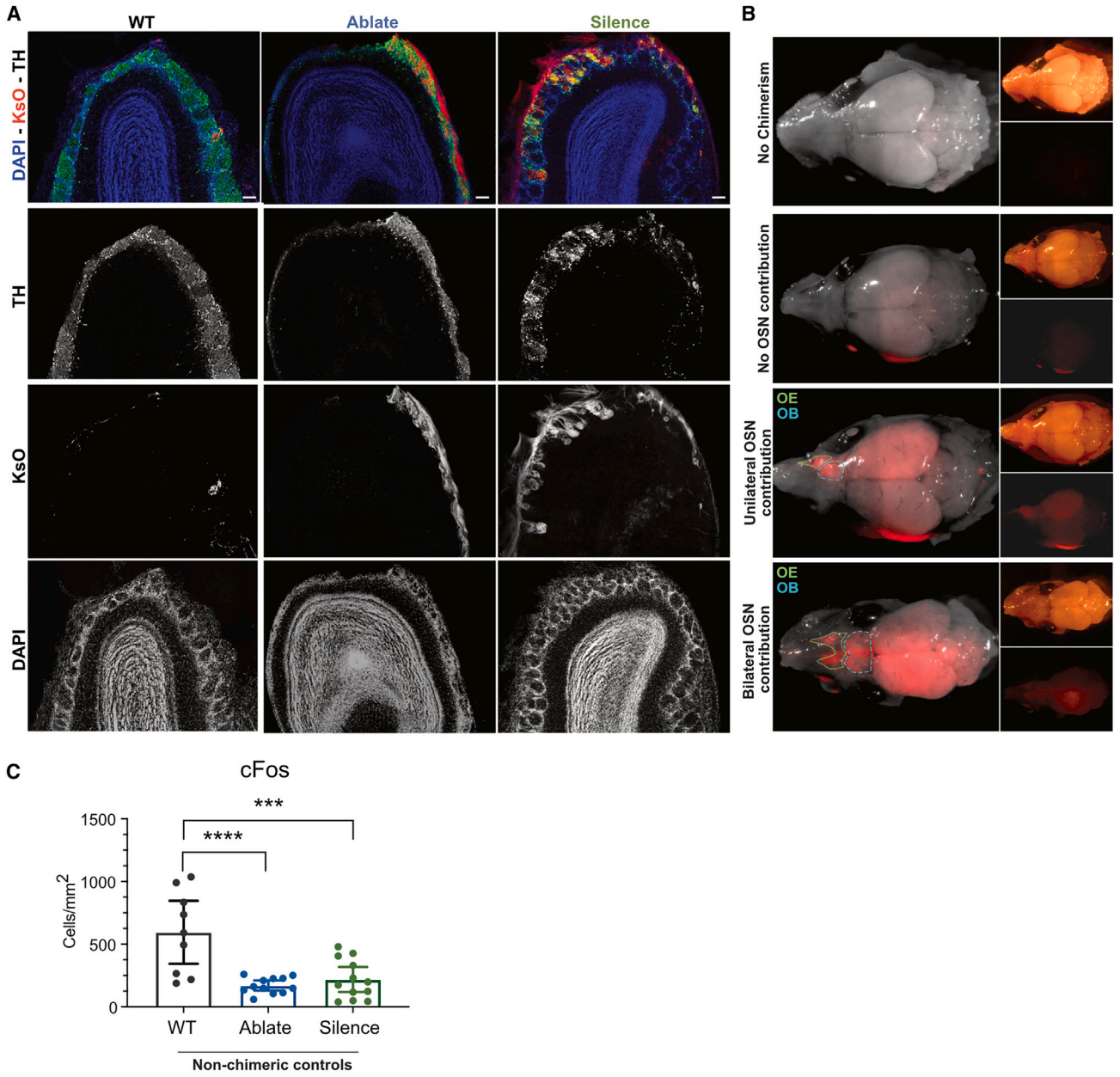

Figure S6. Rat impact on mouse chimera olfactory circuits, related to Figure 6

(A) Rat and mouse glomeruli stained for tyrosine hydroxylase (TH, green), nuclei (DAPI, blue), and rat KsO (red). Scale bars, 100 μm. Images from Figure 6A are reproduced with each channel separated.

(B) Rat mouse chimeras with varying degrees of rat neuron contribution to the olfactory system are shown. The OB and OE are outlined in green and blue, respectively.

(C) Shown are the cells positive for c-Fos per mm^2 for the mice, with rat contribution on the contralateral side. Each dot represents data from one hemisphere for both control hemisphere and rat OSN contribution hemisphere within the same animal. Ablate and Silence models show less c-Fos activation in the mouse PCx. Shown are the cells positive for c-Fos per mm^2 in each mouse model. Data shown are the mean ± 95% CI. Significance was tested by one-way ANOVA. ***$p < 0.0001$, ****$p < 0.0003$.